ISTANBUL TECHNICAL UNIVERSITY ★ GRADUATE SCHOOL

FABRICATION OF MICROMIXERS FOR EFFICIENT ANTIGEN-ANTIBODY BINDING

M.Sc. THESIS

Amenah AL-BARUDI

Department of Nanoscience & Nanoengineering

Nanoscience & Nanoengineering Programme

APRIL 2023

ISTANBUL TECHNICAL UNIVERSITY ★ GRADUATE SCHOOL

FABRICATION OF MICROMIXERS FOR EFFICIENT ANTIGEN-ANTIBODY BINDING

M.Sc. THESIS

Amenah AL-BARUDI
(513191021)

Department of Nanoscience & Nanoengineering

Nanoscience & Nanoengineering Programme

Thesis Advisor: Prof. Dr. Hüseyin KIZIL

APRIL 2023

ISTANBUL TEKNİK ÜNİVERSİTESİ ★ LİSANSÜSTÜ EĞİTİM ENSTİTÜSÜ

VERİMLİ ANTİJEN-ANTİKOR BAĞLANMASI İÇİN MİKRO KARIŞTIRICILARIN ÜRETİMİ

YÜKSEK LİSANS TEZİ

Amenah AL-BARUDİ
(513191021)

Nanobilim & Nanomühendislik Anabilim Dalı

Nanobilim & Nanomühendislik Programı

Tez Danışmanı: Prof. Dr. Hüseyin KIZIL

NİSAN 2023

Amenah AL-BARUDI, a M.Sc. student of İTU Graduate School student ID 513191021, successfully defended the thesis entitled "FABRICATION OF MICROMIXERS FOR EFFIECENT ANTIGEN-ANTIBODY BINDING", which she prepared after fulfilling the requirements specified in the associated legislations, before the jury whose signatures are below.

Thesis Advisor :	**Prof. Dr. Hüseyin KIZIL** Istanbul Technical University	.....
Jury Members :	**Assoc. Dr. Onur ALPTÜRK** Istanbul Technical University	.....
	Prof. Dr. Alper KİRAZ Koç University	.....

Date of Submission : 18 December 2022
Date of Defense : 04 April 2023

To my family and loved ones,

FOREWORD

This thesis was written for my Master's degree in Nanoscience and nanoengineering at Istanbul Technical University. The subject of this thesis is about developing a microfluidic component (Micromixers) that could be used in immnunosensors for early disease recognition and treatment.

I would like to thank my family and loved ones for supporting me through this journey. Their patience, understanding, and encouragement were my guiding torch.

I also extend my gratitude to my supervisor Prof. Dr. Hüseyin KIZIL for his time and patience, and to Dr. Emre ALTINAĞAÇ for his help and support.

This work was supported by TUBITAK under project No. 20AG012.

December 2022 Amenah AL-BARUDI

TABLE OF CONTENTS

Page

FOREWORD ..... **ix**
TABLE OF CONTENTS ..... **xi**
ABBREVIATIONS ..... **xiii**
SYMBOLS ..... **xv**
LIST OF TABLES ..... **xvii**
LIST OF FIGURES ..... **xix**
SUMMARY ..... **xxi**
ÖZET ..... **xxiii**
1. INTRODUCTION **1**
1.1 Literature Review 1
1.1.1 Immunosensors 1
1.1.2 Micromixers 5
1.1.2.1 Passive micromixers 5
1.1.3 Fabrication 10
1.1.3.1 Materials 10
1.1.3.1 Fabrication techniques 12
1.1.4 Electrochemical impedance spectroscopy (EIS) 14
2. DESIGN AND SIMULATION **17**
3. DEVICE FABRICATION **21**
3.1 Silicon Wafer Patterning 21
3.2 PDMS Microfluidic Channel 23
3.3 Electrode Placement 25
4. EXPERIMENTS AND RESULTS **27**
4.1 Materials and Instruments 27
4.2 Ink Test 27
4.3 Optimal PBS Concentration 28
4.4 Impedance of Bare Magnetic Beads and Peptide Bound to Magnetic Beads 29
4.5 Impedance of Free Peptide 32
4.6 Increasing The Hydrophilicity of Microfluidic Channel 33
4.7 The Microfluidic Channel 35
5. CONCLUSION AND RECOMMENTATIONS **39**
REFERENCES **41**
CURRICULUM VITAE **51**

ABBREVIATIONS

2-D	**:** Two Dimensional
3-D	**:** Three Dimensional
AC	**:** Alternate Current
ACEK	**:** Alternate Current Electrokinetics
ACEO	**:** Alternate Current Electroosmotic
ACET	**:** Alternate Current Electrothermal
EIS	**:** Electrochemical Impedance Spectroscopy
PBS	**:** Phosphate Buffer Solution
PDMS	**:** Polydimethylsiloxane
PEB	**:** Post Exposure Bake
PMMA	**:** Polymethylmethacrylate
POC	**:** Point-of-care
SAR	**:** Split and Recombine
SERS	**:** Surface-Enhanced Raman Scattering
SPE	**:** Screen-Printed Electrodes
UV	**:** Ultraviolet

SYMBOLS

μ	**:** Solvent Viscosity
D	**:** Diffusion Coefficient
K_B	**:** Boltzmann's Constant
L_C	**:** Characteristic Length
PE	**:** Peclet Number
RE	**:** Reynolds Number
Ro	**:** Solute Radius
T	**:** Temperature
u	**:** Velocity
v	**:** Kinematic Viscosity
Z, Z_r ,jZ_i	**:** Impedance, Real Impedance, Imaginary Impedance

LIST OF TABLES

Page

Table 1.1 : Microfluidic immunosensors proposed as diagnostic platforms..... **4**
Table 2.1 : Microfluidic channels geometries and dimensions. **18**
Table 2.2 : Reynolds and Peclet numbers. **20**
Table 3.1 : Processes and parameters..... **23**
Table 4.1 : Concentration of bound peptide in TUBITAK samples. **30**
Table 4.2 : The amount of infused species and their flow rates. **36**

LIST OF FIGURES

Page

Figure 1.1 : Concept of parallel lamination with geometric focusing **6**
Figure 1.2 : a) T-shaped micromixer b) Y-shaped micromixer **6**
Figure 1.3 : Concept of sequential lamination micromixer **7**
Figure 1.4 : Concept of flow-focusing micromixer **7**
Figure 1.5 : a) Square obstacles b) Cylindrical pillars c) Repeated curves d) Sharp turns **8**
Figure 1.6 : a) C-shaped micromixer b) L-shaped micromixer **9**
Figure 2.1 : Proposed microfluidic designs. **17**
Figure 2.2 : Microfluidic channels flow simulation. **19**
Figure 3.1 : Comparison between positive and negative photoresists. **22**
Figure 3.2 : Patterned silicon wafer. **22**
Figure 3.3 : Replica molding process. **24**
Figure 3.4 : The fabricated microfluidic systems. **24**
Figure 3.5 : Electrode alignment. **25**
Figure 4.1 : Microscopic images of the inlets and outlets of the fabricated microfluidic channels **28**
Figure 4.2 : Bode plot of different concentrations of PBS **29**
Figure 4.3 : Bode plot of 0.1 mM PBS and 0.1 mM PBS with 0.1 mg magnetic beads. **31**
Figure 4.4 : Bode plot of peptide bound to magnetic beads. **32**
Figure 4.5 : Bode plot of 0.1 mM, bare magnetic beads, free peptide, and TUBITAK samples **33**
Figure 4.6 : Microfluidic channel walls (a) before 0.3% Tween 20 (b) after 0.3% Tween 20 ..... **34**
Figure 4.7 : Recovery of magnetic beads from the microfluidic channel. **35**
Figure 4.8 : Schematic representation of infused species. **35**
Figure 4.9 : Process of magnetic beads extraction and measurement. **36**
Figure 4.10 : Impedance magnitude of the microfluidic channel output. **37**

FABRICATION OF MICROMIXERS FOR EFFICIENT ANTIGEN-ANTIBODY BINDING

SUMMARY

Microfluidic systems are microscale systems that allow the manipulation of fluids inside their channel. They are increasingly gaining interest in many scientific fields owing to their favorable advantages as they can be utilized for many applications. Microfluidic immunosensors are a fast-growing research field, due to the economic nature of microfluidic systems in price, sample volumes, and consumption of time. The fluid flow inside these microsystems can be described as laminar, where the fluid sheets move in parallel to each other. This poses a challenge in microfluidic immunosensing as it hinders the interaction between species in the fluid.

In this study, micromixers were designed and fabricated to enhance the interaction between the immunological species. Several micromixers were designed and simulated using COMSOL Multiphysics software and the three geometries that showed the best mixing were then fabricated. The microfluidic designs were etched on a 3-inch silicon wafer using the photolithography technique and PDMS was subsequently patterned using replica molding techniques and bonded on a glass substrate using the Oxygen plasma bonding method. Interdigitated screen-printed electrodes were purchased and used to carry out electrochemical measurements to assess the binding between the infused species.

Streptavidin magnetic beads and biotinylated peptide were suspended in PBS and infused through the two inlets of the microfluidic channel at multiple flow rates. The two species were allowed to mix inside the microfluidic micromixer before being collected from the outlet. A constant concentration of streptavidin magnetic beads was chosen to mix with different concentrations of the biotinylated peptide at a time. The bound magnetic beads were then immobilized on the surface of the screen-printed electrode using a magnet and impedance measurements were taken.

Preliminary results indicate that the fabricated micromixers were able to induce turbulence in the laminar flow and enhance mixing.

This work was supported by TUBITAK under project No. 20AG012.

VERİMLİ ANTİJEN-ANTİKOR BAĞLANMASI İÇİN MİKRO KARIŞTIRICILARIN ÜRETİMİ

ÖZET

Mikroakışkan sistemler, kanallarının içindeki sıvıların manipüle edilmesine izin veren mikro ölçekli sistemlerdir. Birçok uygulamada kullanılabilmeleri nedeniyle birçok bilimsel alanda giderek daha fazla ilgi görmektedirler. Mikroakışkan immünosensörler, mikroakışkan sistemlerin fiyat, numune hacimleri ve zaman tüketimi açısından ekonomik olması sebebiyle hızla büyüyen bir araştırma alanıdır. Bu mikro sistemlerin içindeki sıvı akışı, sıvıların birbirine paralel hareket ettiği laminar akış olarak tanımlanabilir. Bu, sıvıdaki immünolojik moleküller arasındaki etkileşimi engellediği için algılamada bir zorluk teşkil etmektedir.

Mikroakışkan sistemler, mikro karıştırıcılar gibi sıvıları manipüle edebilen bileşenleri bu sisteme entegre edebilmektedir. İki boyutlu veya üç boyutlu geometriler, üretim tekniğine, maliyete ve uygulamaya bağlı olarak mikro karıştırıcıları üretmek için kullanılabilir. Mikro ölçekte, parçacık hareketini yönlendiren temel kuvvet moleküler difüzyondur ve sıvıda asılı parçacıkların rastgele hareketi ile gerçekleştirilir. Bu mikro bileşenlerin dahil edilmesi, girdaplar ve ikincil akışlar yaratarak sıvı akışında türbülansın ortaya çıkmasına yardımcı olur. Mikroakışkan homojen immünosensörlerde, mikro karıştırıcıların entegrasyonu, immünolojik moleküller arasındaki temas alanını arttırmak, etkileşimlerini arttırmak ve reaksiyon süresini kısaltmak için uygun ve basit bir yol sunar.

Mikro karıştırıcılar aktif ve pasif olarak sınıflandırılmaktadır. Aktif mikro karıştırıcılar türbülansı oluşturmak için harici bir enerji kuvvetine ihtiyaç duyarken, pasif mikro karıştırıcılar geometrik dizaynlar aracılığıyla bunu sağlar. Pasif mikro karıştırıcılarda bariyerlerin, olukların, bölünmüş ve rekombine edilmiş yapıların ve kıvrımlı yapıların kullanılması laminar sıvı akışını bozarak karıştırmayı sağlar.

Mikroakışkan sistemleri üretmek için cam, silikon ve polimerler dahil olmak üzere çeşitli malzemeler kullanılmaktadır. Ayrıca, bu sistemler farklı teknikler kullanılarak da üretilmektedir. Sonuç olarak, malzeme ve üretim tekniğinin seçimi üretim sistemlerinin maliyetine, mevcudiyetine ve uygulamasına bağlıdır.

Bu çalışmanın amacı, antijen-antikor etkileşimini artırmak için verimli iki boyutlu pasif mikro karıştırıcıların tasarlanması ve üretilmesidir. Karıştırma verimliliği, streptavidin manyetik boncukların ve biyotinlenmiş peptitlerin mikrokanal girişlerinden beslenmesiyle elde edilir. Çözelti karışımı kanalın çıkışından toplanır ve empedans ölçümleri alınır.

COMSOL Multiphysics kullanılarak üç mikro karıştırıcı geometrisi tasarlanmış ve simüle edilmiştir. Mikroakışkan kanal içerisindeki karıştırmayı simüle etmek için laminar akış ve seyreltilmiş çözeltinin taşınması arayüzleri kullanılmıştır. Navier-Stokes, difüzyon ve konveksiyon denklemleri, sıvı karışımını simüle etmek için yazılım tarafından çözüldü.

Her iki giriş için 0.008 m/s'lik bir giriş akış hızı ve her giriş için 0 ve 1 mol/L'lik bir molar konsantrasyon ayarlanmıştır. Çıkışta ortalama 0.5 mol/L molar konsantrasyon elde edilerek etkili karıştırma gözlemLendi. Mikroakışkan kanalların genel tasarımı iki girişten oluşmaktadır: Biri streptavidin manyetik boncuklar için diğeri biyotinlenmiş peptitler içindir, ayrıca bir mikro karıştırıcı ve bir çıkış bulunmaktadır. Streptavidin manyetik boncukların girişi için iki farklı geometri tasarlanmasının sebebi antijen-antikor etkileşimini arttırmak ve manyetik boncukların kanal içerisinde dağılımını sağlayıp dönmesini sağlamaktır. Tüm tasarımLaın kanal yüksekliği 50 mikrometredir ve genel genişlik 200 mikrometredir ve en boy oranı 0.2'dir. Genişleme-daralma ve asimetrik kare dalga olmak üzere iki karıştırma geometrisi önerilmiştir. Bu geometriler akışta türbülans oluşturarak ve temas alanını arttırarak karışmayı sağlar.

Mikroakışkan sistemler iki adımda üretilmektedir. 1) Fotolitografi tekniği ile silikon kalıbın modellenmesi, 2) replika kalıplama tekniği ile PDMS mikrokanallarının üretilmesi.

Silikon kalıbın oluşturulması için, mikroakışkan kanal tasarımları, fotolitografi kullanılarak 4 inçlik silikon waferlar üzerinde modellendi.

Mikroakışkan tasarımları silikon wafera aktarmak için önceden sipariş edilen desenli bir asetat maskesi kullanıldı. Silikon wafer yıkandı ve hazırlandı, ardından SU-8 3050 negatif fotorezist, wafer üzerinde 50 mikrometrelik bir kalınlık elde etmek için döndürülerek kaplandı. Kaplanmış silikon wafer, 95 ˚C'de 15 dakika boyunca sıcak plaka üzerinde tutuldu. Soğutulduktan sonra, 1 mikrometreye kadar çözünürlük elde etmek için asetat maskesi doğrudan kaplanmış silikon wafer üzerine yerleştirildi ve UV ışık kaynağına (260-325 nm) SUSS Microtec (MA6/BA6) makinesi kullanlarak10 saniye boyunca maruz bırakıldı. Desenlenmiş wafer 65 ˚C'de 1 dakika ve sonrasında 95 ˚C'de 5 dakika boyunca sıcak plaka üzerinde bekletildi. Silikon wafer içerisinde SU-8 geliştiricisinin bulunduğu çözeltiye daldırıldı ve desenler net bir şekilde görünür oluncaya kadar yaklaşık 8 dakika kadar bu çözelti banyosunun içinde çalkalandı. Son olarak silikon wafer, dayanıklılığı arttırmak için 150 ˚C'de 20 dakika boyunca sıcak plaka üzerinde tutuldu.

PDMS mikroakışkan kanalları replika kalıplama tekniği kullanılarak üretildi. PDMS, katılaştırma maddesi ile 10:1 ağırlık/ağırlık oranında karıştırıldı ve desikatör kullanılarak 20 dakika boyunca gaz giderme işlemi uygulandı. Daha sonra, PDMS hazırlanan silikon kalıba döküldü ve katılaşması için 90 ˚C'de 20 dakika sıcak plaka üzerinde ısıtıldı. Katılaştıktan sonra, PDMS, girişleri ve çıkışı delmek için kalıptan dikkatlice soyuldu ve bir cam yüzeyin üstüne sığacak (55 mm x 27,5 mm) şekilde tabakalar halinde kesildi. Mikrokanal girişleri ve çıkışı delindi ve PDMS, oksijen plazma bağlanması yöntemiyle bir cam substrat yüzeyine bağlandı. Plazma cihazının içerisi önce vakumLandı, ardından kapağı kapatılmadan önce 50 saniye boyunca oksijenin ortam içerisine dağılmasına izin verildi. Plazma makinesi daha sonra açıldı ve yüksek ayara getirildi. Mora yakın bir renk değişimi gözlemLendikten sonra, PDMS ve cam substratlar çıkarılıp bir araya getirilmeden önce 50 sn kadar plazmaya maruz bırakıldı.

10 mikrolitre streptavidin manyetik boncukları ve farklı konsantrasyonlarda biyotinlenmiş peptidler, PBS içinde süspanse edildi ve girişlerden farklı akış hızlarında verildi. Çözelti çıkıştan alınmadan önce iki sıvının mikro karıştırıcı içerisinde karışması sağlandı. Karıştırıldıktan sonra, manyetik boncuklar bir mıknatıs aracılığıyla karışımdan ayrıldı ve PBS içinde yeniden süspanse edildi.

Streptavidin manyetik boncuklarının empedans ölçümLeri, boncukların PBS içinde süspanse edilmesi ve daha sonra bir mıknatıs kullanılarak elektrot üzerinde hareketsizleştirilmesiyle alınan karıştırmadan önce ve sonra alınmıştır.

Empedans ölçümLerini gerçekleştirmek için ”Metrohm”dan DropSens DRP-GIDEAU10 altın birbirine geçmiş ekran baskılı elektrotlar satın alınmıştır.

İki pürüzsüz PDMS levhası arasına bir elektrot yerleştirildi, üst tabaka elektrodun algılama bölgesinin üstünde hizalanmış bir açıklığa sahipti ve burada toplanan numuneler ölçümler için yerleştirildi. Ön sonuçlar, fabrikasyon mikro karıştırıcıların laminer akışta türbülansı indükleyebildiğini ve karıştırmayı geliştirebildiğini göstermektedir.

Bu çalışma TÜBİTAK tarafından 20AG012 nolu proje kapsamında desteklenmiştir.

1. INTRODUCTION

Microfluidic systems have attracted significant attention in the past few years in biomedical analysis due to their economical and analytical advantages. Traditional immunosensors rely on the diffusion coefficients of reactants, leading to slow reactions. The flexible design of microfluidic systems eases the integration of micromixers that facilitate chemical and biological reactions inside the microchannel by disturbing the laminar flow in microfluidic systems with small Reynolds numbers. These miniaturized systems offer high specific area, increasing contact medium between fluids and leading to fast reaction rates.

1.1 Literature Review

The development in analysis methods had led to an increase in the number of diagnostic analytes. The capture and quantification of these biomarkers is the first step in disease diagnosis and treatment, therefore numerous sensing technologies are rapidly developed [1].

In recent years, the integration of biosensors and microfluidic devices has attracted significant attention owing to their advantages [2]. The use of microfluidic systems as quantitative immunological devices offers the use of small sample volume, multianalyte detection, increased sensitivity, incorporation of micro-flow components, automation, high surface-to-volume ratio, and short analysis time by decreasing diffusion distance when compared to conventional methods [2], [3].

1.1.1 Immunosensors

Heterogenous and homogenous immunosensors are well-suited for integration with microfluidic systems. In heterogenous biosensors, the detection probe (antibody) is immobilized on the surface of the sensor, whereas in homogenous biosensors, the detection probe (antibody) and sample (antigen) are mixed, and the signal is measured from the mixture for detection [1].

There are three main detection methods used in microfluidic immunosensors; fluorescence, electrochemical, and surface plasmon resonance [3].

The incorporation of biosensors with microfluidic platforms offers a number of advantages such as achieving a lower detection limit, high accuracy, providing biological reactors, fast detection, sample volume manipulation, automation, and affordability [4].

Microfluidic biosensors can be constructed in a relativity simple design, where inlets are connected to a long microchannel that is positioned on top of a sensing platform and the sample is generally driven through the microchannel by applying pressure [5].

Due to the miniaturized size of microfluidic systems, the movement of dispensed particles inside the microfluidic channel is governed by molecular diffusion [6]. This slow movement and mixture of particles is a challenge that hinders immunological reactions in immunosensors.

In heterogenous immunosensors, the slow movement of particles leads to the formation of a diffusion boundary layer on the reaction surface that inhibits the interaction between the dispensed antigen and the immobilized antibody leading to increased reaction time [7], [8].

To overcome this limitation, different approaches have been utilized to disrupt the diffusion boundary layer such as alternate current electrokinetics (ACEK) techniques including AC electrothermal (ACET) effect or AC electroosmotic (ACEO) or the incorporation of dielectrophoresis [9]–[11], flow deformation with obstacle placement [12], [13] and the use of confining secondary flow [14].

Several studies have been published that utilize the above-mentioned techniques to increase the detection limit of analytes [15]–[19]. Although heterogeneous microfluidic immunosensors offer many advantages such as high sensitivity and selectivity [20], they are limited by the formation of diffusion double layer, cost, separation, and sample preparation. Despite the different techniques that have been proposed to solve the problem of diffusion boundary layer formation, their utilization adds complexity to the design, fabrication, and operation of these devices.

On the other hand, homogenous biosensors do not require sample perpetration and are easier to operate, affordable, enable antibody immobilization of micro/nanospheres, and are effective for detection in small complex samples making them ideal for point-

of-care (POC) sensor applications [1], [21]. Detection in homogenous immunosensors depends on the formation of antigen-antibody complexes by mixing [22]. However, owing to the small scale of microfluidic systems, the viscous forces of the fluid inside the microchannel are stronger than the inertial forces characterizing the flow as laminar [3]. Laminar flow is represented by the movement of fluid in parallel sheets, where no mixing occurs [23]. The characteristic of fluid flow can be determined by a dimensionless number, called the Reynolds number [24]. In the microscale, laminar flow is defined when the Reynolds number is less than the critical value of 1500. As a result of the dominant viscous effect, the mixing inside the microfluidic channel is dependent entirely on molecular diffusion leading to longer reaction time and requiring longer microfluidic channels [25].

The laminar flow, therefore, reduces the chances of the biological reaction between antigen-antibody, reducing the complex formation and therefore detection. This can be overcome by utilizing a micro-flow component (a micromixer) [26].

For optimal micro- to nano-fluid manipulation, several features need to be considered such as the fabrication material, aspect ratio, and the integration of micro-flow components for the intended function/functions. One of the most important micro-flow components that can be easily integrated into the microfluidic channel is a micromixer [2], [27]. The integration of micromixers induces turbulence inside the microfluidic channel by disturbing the laminar flow, enhancing mixing [22]. Therefore, the incorporation of micromixers in homogenous immunosensing devices can increase the formation of immunological complexes, reducing reaction time and enhancing the sensitivity of the device. Several microfluidic immunosensors were designed for the detection of many disease-related biomarkers, a number of which are listed in (Table 1.1).

Table 1.1 : Microfluidic immunosensors proposed as diagnostic platforms.

Disease	Biomarker	Detection method	LOD	Rf.
Prostate cancer	Prostate-specific antigen (PSA)	Surface-enhanced Raman scattering (SERS)	0.01 ng/mL	[28]
Cancer	Alpha-fetoprotein (AFP) and c-reactive protein (CRP)	Fluorescence	1 pg/mL	[29]
Diabetes	Insulin	Chemiluminescence	$4x10^{-10}$ mol/L	[30]
Breast cancer	Cancer Antigen (CA153, CA125) and Carcinoembryonic Antigen (CEA)	Surface-enhanced Raman scattering (SERS)	0.01 U/mL, 0.01 U/mL and 1 pg/mL	[31]
Inflammation	C-reactive protein (CRP), Procalcitonin (PCT), and Interleukin-6 (IL-6)	Chemiluminescence	1.25–40 µg/mL, 0.4–12.8 ng/mL, and 50–1600 pg/mL	[32]
Complications of Gastrointestinal fistula	C-reactive protein (CRP) and Prealbumin (PAB)	Electrochemical	5 pg/mL and 10 pg/mL	[33]
Acute myocardial infarction	Cardiac troponin I (cTnI)	Electrochemical	0.05 ng/mL	[34]
Prostate Cancer	Prostate-specific Antigen (PSA)	Electrochemical	2 pg/mL	[35]
Alzheimer's	A Disintegrin And Metalloprotease 10 (ADAM10)	Electrochemical	0.35fg/mL	[36]
Aspergillosis	Galactomannan (GM)	Fluorescence	0.07ng/mL	[37]

1.1.2 Micromixers

Micromixers are microscale components that induce the mixing of at least two different phases, and they are characterized by miniature channel dimensions of 100-500 μm. Mixing in the microscale is achieved by molecular diffusion, advection, and Taylor dispersion. Molecular diffusion is realized by the random movement of suspended particles, advection is realized by the movement of particles due to the fluid motion, and Taylor dispersion is the resulting advection of several velocities. The main challenges that face the mixing process in the microscale are particle suspension due to the small diffusion coefficient and laminar flow that is caused by the dominant viscous effect. The utilization of chaotic advection can help overcome the challenges of the microscale [38], Thus optimizing the design and operation of micromixers can greatly affect the mixing process.

Micromixers can serve as microreactors for chemical or biological reactions. The innate advantages offered by their microscale features offer several advantages that facilitate reactions. The superiority of utilizing micromixers as microreactors are owed to their ease of integration, fabrication, operation, and large surface-to-volume ratio resulting in affordable reactors and efficient reactions [39].

Micromixers are divided into two categories, passive and active mixers [24]–[26], [40]. While passive micromixers required no external energy and rely on channel geometry to manipulate the fluid flow, active mixers require external energy in form of acoustic, magnetic, electrical, thermal, or pressure. Although active micromixers provide better control over the mixing inside the microfluidic channel [26], passive micromixers offer ease of fabrication, integration, and operation [41].

1.1.2.1 Passive micromixers

Passive micromixers achieve homogeneous mixing by relying on molecular diffusion and chaotic advection [6]. Since they do not require an external source of energy, the channel geometry can be manipulated to achieve the desired effect. Passive micromixers can either be 2-dimensional or 3-dimensional depending on the desired function and production technique [40]. According to the main transport phenomena that result in mixing, passive micromixers can be categorized into two categories: a) bulk mass transfer micromixers and b) chaotic advection micromixers [38], [42], [43].

A) Bulk mass transfer micromixers

These micromixers rely entirely on molecular diffusion to realize mixing. Molecular diffusion is a physical constant that is dependent on molecule and solvent properties. Molecular defusion is described as seen in equation 1.1.

$$D = \frac{k_B T}{6\pi\mu R_0} \quad (1.1)$$

Where μ is solvent viscosity, R_0 is the solute radius, K_B is Boltzmann's constant, and T is the temperature in kelvin. The optimal method to enhance molecular diffusion is by adapting certain geometries that reduce the striation thickness of the solvent/solvents.

Parallel Lamination Micromixers: These micromixers rely on splitting the inlet streams into a number (n) of smaller streams and then recombining them in one channel as shown in (Figure 1.1). This lamination reduces the striation thickness, decreasing the diffusion distance between the fluid layer and increasing the contact area. The simplest type of parallel lamination micromixer is the T or Y type. T or Y micromixers use a two-inlet design to laminate two streams and join them in one channel as seen in (Figure 1.2). Obtaining a shorter mixing path can be achieved by narrowing the main mixing channel [44].

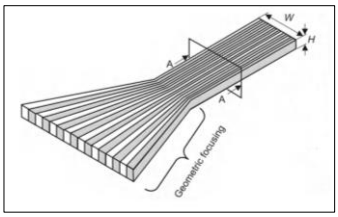

Figure 1.1 : Concept of parallel lamination with geometric focusing [38].

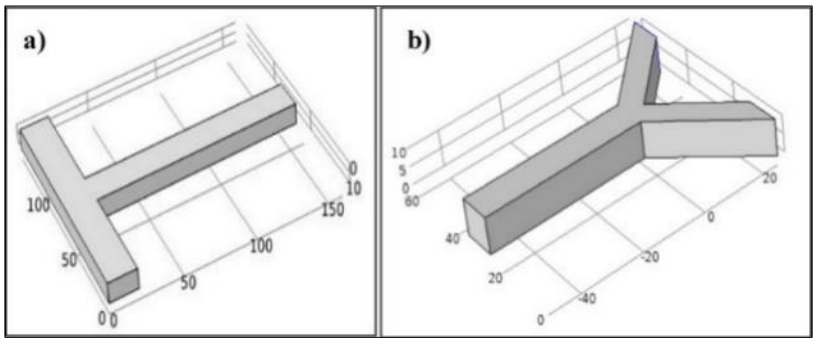

Figure 1.2 : a) T-shaped micromixer b) Y-shaped micromixer [45].

Sequential Lamination Micromixers: Can also be referred to as Split and Recombine micromixers (SAR). These micromixers split the primary laminated stream into secondary streams before rejoining them again as demonstrated in (Figure 1.3).

When compared to parallel lamination micromixers, SAR similarly brings down the diffusion distance and increases contact but they present the advantage of faster mixing for the same mixing area. Generally, SAR micromixers require an out-of-plane design and fabrication but a novel planar laminating passive micromixer was developed by incorporating an in-plan split and recombine structure combined with pattering the channel floor to induce flow rotation to achieve efficient mixing [46].

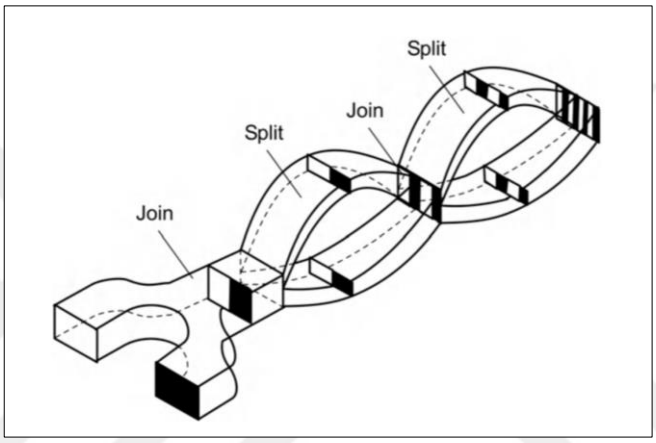

Figure 1.3 : Concept of sequential lamination micromixer [38].

Flow Focusing Micromixers: These micromixers use three inlets to hydrodynamically focus a stream as seen in (Figure 1.4). These micromixers require a long microchannel to focus the flow in the horizontal direction, reducing the fluid width and therefore the diffusion path. The inlet streams can have the same or different viscosities depending on the desired effect and desired sample flow velocity.

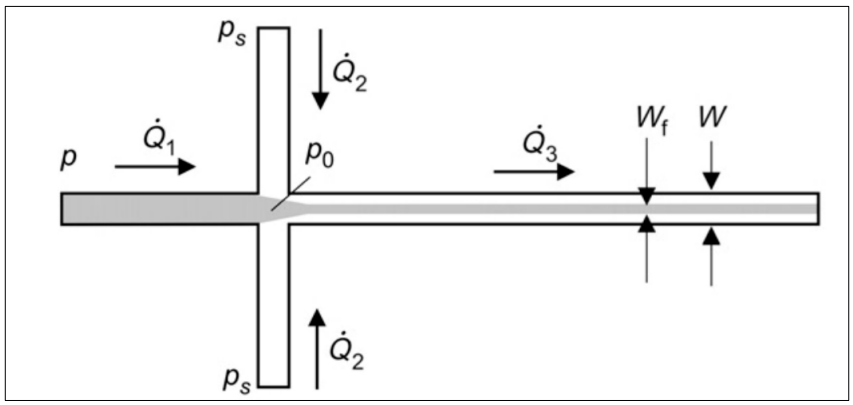

Figure 1.4 : Concept of flow-focusing micromixer [38]**.**

B) Chaotic advection micromixers

Advection is the transport of solute due to the movement of solvent. Chaotic advection micromixers rely on variations in the microchannel geometry and the presence of grooves or obstacles to realize mixing through the stretching and folding of the flow. For example, at a high Reynolds number, a T-type micromixer incorporated with square obstacles alternating along the channel wall would cause the formation of secondary flows generating flow-disturbing vortices [47]. Cylindrical pillars placed in the flow path can enhance mixing due to inertial forces and the change in flow direction [48]. The obstacle placement can further enhance mixing if it's asymmetrical. Repeated curves [49], and sharp turns [50] were also reported to result in chaotic advection at high Reynolds numbers. Several chaotic mixers are illustrated in (Figure 1.5).

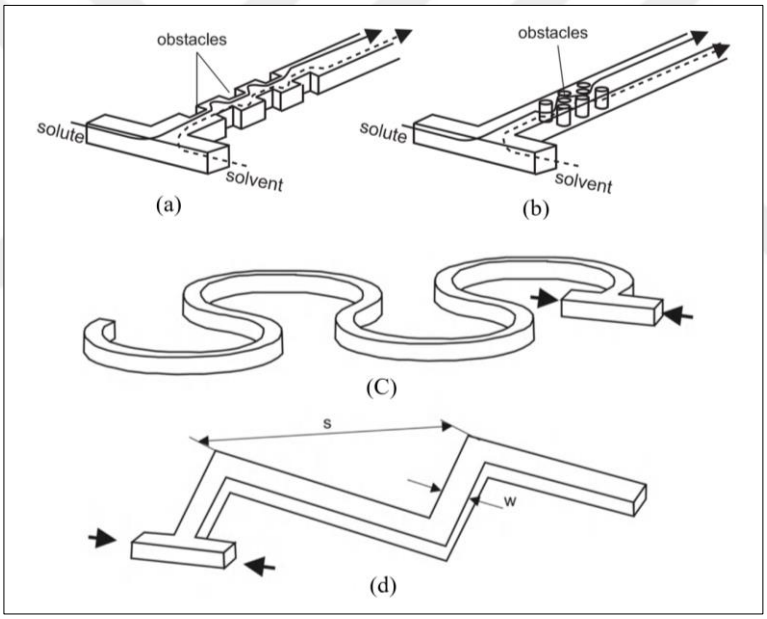

Figure 1.5 : a) Square obstacles b) Cylindrical pillars c) Repeated curves d) Sharp turns [38].

At intermediate Reynolds numbers, 3-D interconnected shapes were investigated for mixing. C-shaped serpentine and L- shaped 3-D channels were reported to enhance mixing [51], [52] as shown in (Figure 1.6). Other variations to the 3-D serpentine micromixer were also investigated; advection serpentine mixer with F-shaped geometries for lamination [53] and the modification of the recombination region of the F-shaped geometry to further enhance mixing performance [54]. Another chaotic micromixer design incorporates ridges on the channel base. The bas-relief structures

produced effective mixing at low Reynolds numbers [43]. Rhombic geometry with flat edges was proposed for high-throughput applications due to the enhanced vortex formation at high Reynolds numbers [55].

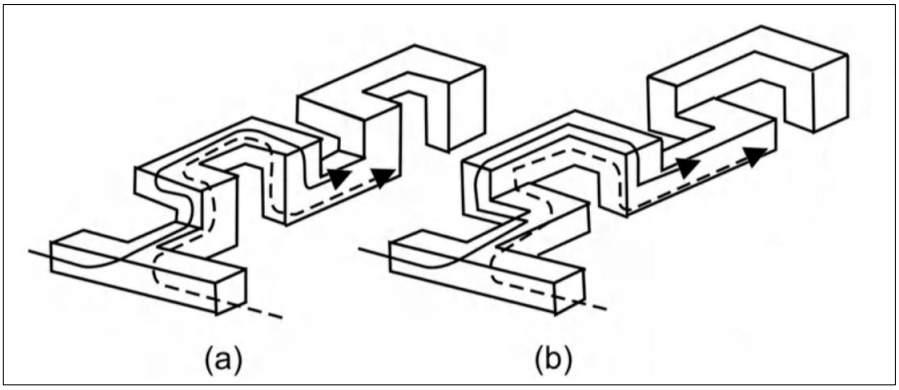

Figure 1.6 : a) C-shaped micromixer b) L-shaped micromixer [38].

Spiral and F- shaped micromixers are reported to cause the formation of dean vortices that enhance mixing at low Reynolds numbers [56], [53].

Chaotic advection micromixers can be designed in various shapes and geometries by changing the wall geometry, obstacle placement, expansion-constriction, and flow recycling can be done by incorporating a number of different mixing geometries altogether [24], [38], [40].

Passive micromixers have been utilized in microfluidic platforms to produce rapid and efficient results in biosensing applications. A 3-D Tesla micromixer has been utilized to enhance the antigen-antibody binding for the detection of lung cancer cells at a sample concentration of 10^2 cells/μL [27]. Another microfluidic biosensor for the detection of the foodborne pathogen of S. Typhimurium bacteria incorporated a 3-D staggered asymmetric herringbone for mixing of samples and followed by a serpentine incubation channel to provide enough time for complex formation. This microfluidic chip design was adapted to enhance mixing and improve sensitivity and provide a detection limit of 73 CFU/mL [57]. Multiple micromixer designs have been tested for the detection of the antibacterial drug Sulfadimethoxine. A 3-D wavy line pattern showed the most efficient mixing and was chosen for the homogenous aptamer-based assay and a limit of detection of 4pg/mL was obtained [58]. A focusing micromixer was designed for microfluidic cytometry. The microchannel included 4 inlets, two inlets were designated for the components to be mixed and the other two inlets were designated for the sheath flow. This design enhances the mixing of the components by

reducing the fluid width and enhancing diffusion and achieved complete mixing of the two components [59]. A laminar split and recombine micromixer was proposed and investigated for the preparation and mixing of blood samples.

The proposed micromixer contained eclipsed-shaped micropillars to split the main flow into two smaller flows before recombining again. The investigation was carried out using the finite element method, COMSOL Multiphysics. The results indicate that the incorporation of the eclipse-shaped micropillar enhances the mixing efficiency of T- shaped mixers with a mixing efficiency of more than 80% at low Reynolds numbers [60]. A novel pump-free SERS-microfluidic homogenous biosensor for the detection of prostate-specific antigen was developed. winding-shape geometry was embodied through the microfluidic channel to enhance the antigen-antibody binding by increasing contact between solutions through chaotic advection. This novel system was able to achieve a detection limit of 0.01 ng/mL [28]. Although 3-D micromixers create better secondary flows that lead to vortex formation that produce more efficient mixing, 2-dimensional micromixers are easier to fabricate and are more economical [58].

1.1.3 Fabrication

Microfluidic devices can be fabricated through a variety of methods each with advantages, disadvantages, and the preferred fabrication material. The choice of the method relies greatly on the desired characteristics of the fabricated microfluidic device and its application [61].

1.1.3.1 Materials

The first thing to consider before deciding on the fabrication technique is the material. In the micro world, the properties of the materials are amplified and can greatly affect the outcome of the product [62].

A- Metals: Aluminum, copper, iron, and their alloys can be used to fabricate microfluidic devices [63]. They offer several advantages such as durability against extreme conditions, accessibility, and affordability. Metallic microfluidic systems act as microreactors for the fabrication of nanomaterials [64].

B- Silicon: One of the earliest materials used for the fabrication of microfluidic systems. Although silicon offers the flexibility of design and micromachining, silicon use in fabrication is limited due to its fragility, price, and complications in incorporating functional components into the device [65], [66]. Silicon microfluidic systems are utilized in many biological applications [65].

C- Glass: Transparency, rigidity, biocompatibility, and durability has made glass one of the most popular materials for microfluidic fabrication but despite these properties, glass micromachining is troublesome and expensive. Glass microfluidics are used as microreactors for nanomaterial synthesis and biological applications [65], [67]–[69].

D- Ceramics: Although ceramics possess strength against harsh chemicals and conditions and unique surface properties, they are not preferred in the fabrication of microfluidic systems due to their porosity and delicacy [65], [68].

E- Paper-based: Paper-based microfluidics were proposed as a feasible and more economical alternative to other materials in disposable point-of-care diagnostics [70]. They are porous, biocompatible, easily modified, and affordable but their use is still limited due to their mechanical strength [71].

F- Polymers: The choice of fabrication materials has shifted from silicon and glass to polymers due to their utility and flexibility of fabrication. The attraction of polymer use in the fabrication of microfluidics systems stems from their favorable properties such as transparency, chemical stability, biocompatibility, and surface tension.

The most commonly used polymers in microfluidic fabrication include polydimethylsiloxane (PDMS), an elastomer, and polymethylmethacrylate (PMMA) a thermoplastic [61], [72]. PDMS is affordable, easily manipulated and molded, biocompatible, transparent, and highly elastic [65], [73]. These properties make PDMS an attractive fabrication material in biological applications such as cell culturing, biomedical diagnostics, and cell screening [62], [74]. PMMA owns similar properties to PDMS in addition to the advantage of better solvent compatibility and no molecular adsorption [71], therefore, PMMA is often used for the fabrication of organ-on-a-chip devices.

The mentioned materials can be incorporated with each other in order to fabricate hybrid microfluidic devices to harvest the desired properties of both materials [75].

1.1.3.2 Fabrication techniques

A variety of fabrication techniques can be utilized to produce microfluidic devices. The choice of the technique depends on multiple factors such as the cost of fabrication, availability, and the choice of the material for the desired application [61]. Below is a summary of the most common fabrication methods.

A- Micromachining:

Micromachining techniques usually involve the use of glass or silicon as fabrication materials due to their rigidity and the use of harsh and corrosive chemicals. Micromachining includes wet and dry etching, photolithography, electron beam lithography, and other techniques [76]. Wet etching can be described as the use of an etchant chemical that removes material to reveal the microfluidic pattern in the solid material. Dry etching can be used to etch the network or pattern of micromixers. Wet etching however uses etchant gases or plasma to remove material. Dry etching can be further categorized into physical dry etching, chemical dry etching, and physical-chemical etching. The best feature resolution can be achieved with plasma dry etching and it is preferred over wet etching for pattering transparent material although it is a slower process [38], [77].

Photolithography is used to transfer the microfluidic pattern onto a substrate through a mask to produce 2-D patterns and is commonly used in the fabrication of micromixers due to its simplicity and rapid prototyping. Photolithography consists of three general steps: the positioning of the mask over the photoresist-covered substrate, UV exposure for pattern transfer, and development for photoresist removal to reveal the pattern [38]. Another micromachining technique is electron beam lithography where accelerated electrons bombard the resist layer and deposit their energy [78]. This technique is preferred over the accessible photolithography technique due to the small features produced (as low as 20nm) and rapid fabrication [79].

B- Replica molding:

Replica molding or soft lithography is one of the most used techniques in the fabrication of medical devices [80]. This technique involves the use of a silicon wafer master patterned with the microfluidic design to pattern an elastomeric material like PDMS. The process starts with creating the silicon master with photolithography, pouring the elastomer (PDMS) on top of the master, curing and peeling off the material to reveal the microfluidic pattern. Using this method can produce high-resolution molds and can be used to produce 3-D devices by assembling multiple layers on top of each other [38], [61], [76].

C- Embossing:

This technique involves the use of thermoplastic material such as PMMA that is patterned against a stamp using pressure and heat. This method is easy, uncomplicated, and cheap. The most complicated or time-consuming part of this method is the fabrication of the stamp from micromachined silicon or metal electroforms. Then, the thermoplastic material is placed in a hydraulic press, and by applying heat and pressure the material is embossed with the stamp and a vacuum can be applied to eliminate air bubbles between the material and the stamp [38], [61], [76].

D- Injection molding:

like embossing, inject molding utilizes silicon and metal molds. This method is limited to thermoelastic materials that are injected into the cavity of the mold to produce the desired patterns. The process starts with heating the material inside a barrel to melt it. After melting, the material is injected into the mold cavity under high pressure. To maintain the shape of the material and release it from the mold, pressure is maintained while the temperature is dropped. This method is economical, precise, and simple with one major drawback being the fabrication of the molds. Several factors can affect the quality of produced geometries such as the quality of the mold, the properties of the material, temperature, pressure, and the residence time [38], [61], [76].

1.1.4 Electrochemical impedance spectroscopy (EIS)

With the development in MEMS fabrication and the rapid demand for cost-effective diagnostics, electrochemical impedance spectroscopy has gained interest in the detection of biomarkers in point-of-care (POC) applications [81]. EIS offers multiple advantages such as high sensitivity, non-destructive, and multianalyte label-free detection [82]. Impedance is the resistive force to an electrical current in AC circuits, it can be described as "the complex ratio of voltage and current in an AC circuit" [83].

The electrical current flows at various frequencies through a cell, in the case of the microfluidic biosensor, it is the detection chamber and electrode. The different frequencies applied have different phase angles that result in a capacitive or inductive effect [82]. After applying the current, its response is measured and used to obtain real, imaginary, phase angle, and complex impedance [84] as seen in equation 1.2.

$$Z(j\omega) = Zr(\omega) + jZi(\omega) \quad (1.2)$$

Where $Z(j\omega)$ is the complex impedance, $Zr(\omega)$ is the real impedance and $jZi(\omega)$ is the imaginary impedance. Impedance data can be plotted as imaginary and real impedance in the Nyquist diagram to obtain resistance, charge transfer resistance, and Warburg impedance. Impedance and phase angle and frequency can also be plotted in the Bode diagram to obtain information about the capacitive or inductive effects of the electrochemical cell [82] [85].

Electrochemical impedance spectroscopy can be categorized into two categories, faradaic and non-faradaic. In faradaic sensors, redox probes are present in the solution and the measured impedance is related to the charge transfer of the reactive species on the surface of electrodes [86]. Non-faradaic sensors however do not require the presence of redox probes. Instead, non-faradic impedance is related to the insulating effect of the target molecule when it binds to the surface of the electrode [87]. Although faradic sensors are superior in sensitivity in comparison to non-faradaic sensors, the latter is more suitable for point-of-care applications [88].

Electrochemical impedance spectroscopy can be used to measure and evaluate antigen-antibody binding in real time [19], [89], [90]. The impedance measurement changes are the target molecule binds to the immobilized magnetic beads on the surface of the sensing electrode. In this study, the unbound streptavidin-coated magnetic beads are immobilized on the electrode surface using a strong magnet, and impedance

measurements are carried out as Z before binding the biotinylated peptide. Impedance measurements are repeated after the binding to peptide to magnetic beads to obtain Z after binding.

To obtain the magnetic beads and peptide binding measurements equation 1.3 is solved:

$$\Delta Z / Z_{\text{Reference}} = (Z_{\text{After Binding}} - Z_{\text{Before Binding}}) / Z_{\text{Before Binding}} \quad (1.3)$$

2. DESIGN AND SIMULATION

In this chapter, the design and dimensions of the proposed microfluidic micromixers are discussed.

The microfluidic channels were designed to optimize the interaction between biological species. Several mixing-unite geometries were designed and repeated throughout the microfluidic channel. In total 12 microfluidic channels were designed and simulated using COMSOL Multiphysics 5.6 software.

The general design of the microfluidic channels consisted of two inlets: one for the streptavidin-coated magnetic beads and one for the biotinylated peptide, a micromixer, and one outlet. Two geometries for the inlet of the magnetic beads were designed to enhance the dispersion and rotation of the functionalized magnetic beads which might enhance the interaction between species.

3 designs were chosen to be fabricated based on their simulation results as seen in Figure (2.1).

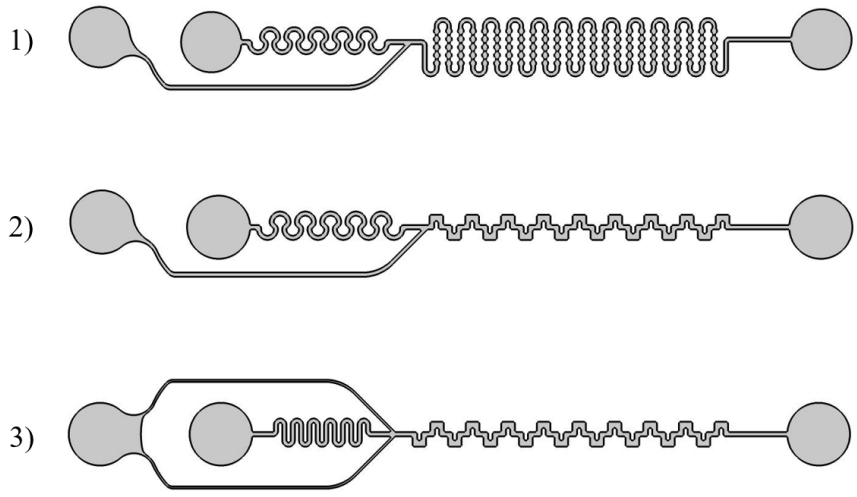

Figure 2.1 : Proposed microfluidic designs.

All designs had a channel height of 50 μm and general width is 200 μm with a small aspect ratio of 0.2, geometries and their specifications are indicated in (Table 2.1). The

choice of the height and width of the channel was made to decrease the diffusion distance while keeping in mind the limitations of the fabrication technique.

Two mixing geometries were proposed for the design of the micromixers, expansion-constriction, and asymmetric square wave. Consecutive expansion-constriction geometries induce turbulence in the flow and increase the interface area between the infused fluids by condensing and then separating the flow at the expansion regions leading to vortex formation. While the mixing in the asymmetric path micromixer is caused by the formation of small eddies at the curves of the channel which cause turbulence.

Table 2.1 : Microfluidic channels geometries and dimensions.

Microfluidic channel	Number of inlets	Mixing geometry	Dimensions
	1 for each species		300 µm expansion, 100 µm constriction
	1 for each species		Asymmetric path 200, 225, 300 µm
	1 for magnetic beads, 2 for protein/peptide		Asymmetric path 200, 225, 300 µm

Laminar flow and transport of diluted solution interfaces were used to simulate the mixing inside the microfluidic channel. Navier-Stokes, diffusion, and convection equations were solved by the software to simulate fluid mixing. An inlet flow velocity of 0.008 m/s was set for both inlets and a molar concentration of 0 and 1 mol/L was set for each outlet. COMSOL Multiphysics Simulation results demonstrated effective mixing by measuring a molar concentration of 0.5 mol/L at the microfluidic channel outlet indicated by the color green as seen in (Figure 2.2). Simulation results also indicated that these geometries can produce sufficient mixing at a low Reynolds number. There are two characteristic dimensionless numbers to consider in microfluidics, the Reynolds number, and the Peclet number. Reynolds number

corresponds to The flow rate, it is the ratio between the inertial and viscous forces. Whereas the Peclet number is the ratio between convection and diffusion.

In micromixers, Low Reynolds numbers characterize the flow as laminar, and high Peclet number >> 1 is required.

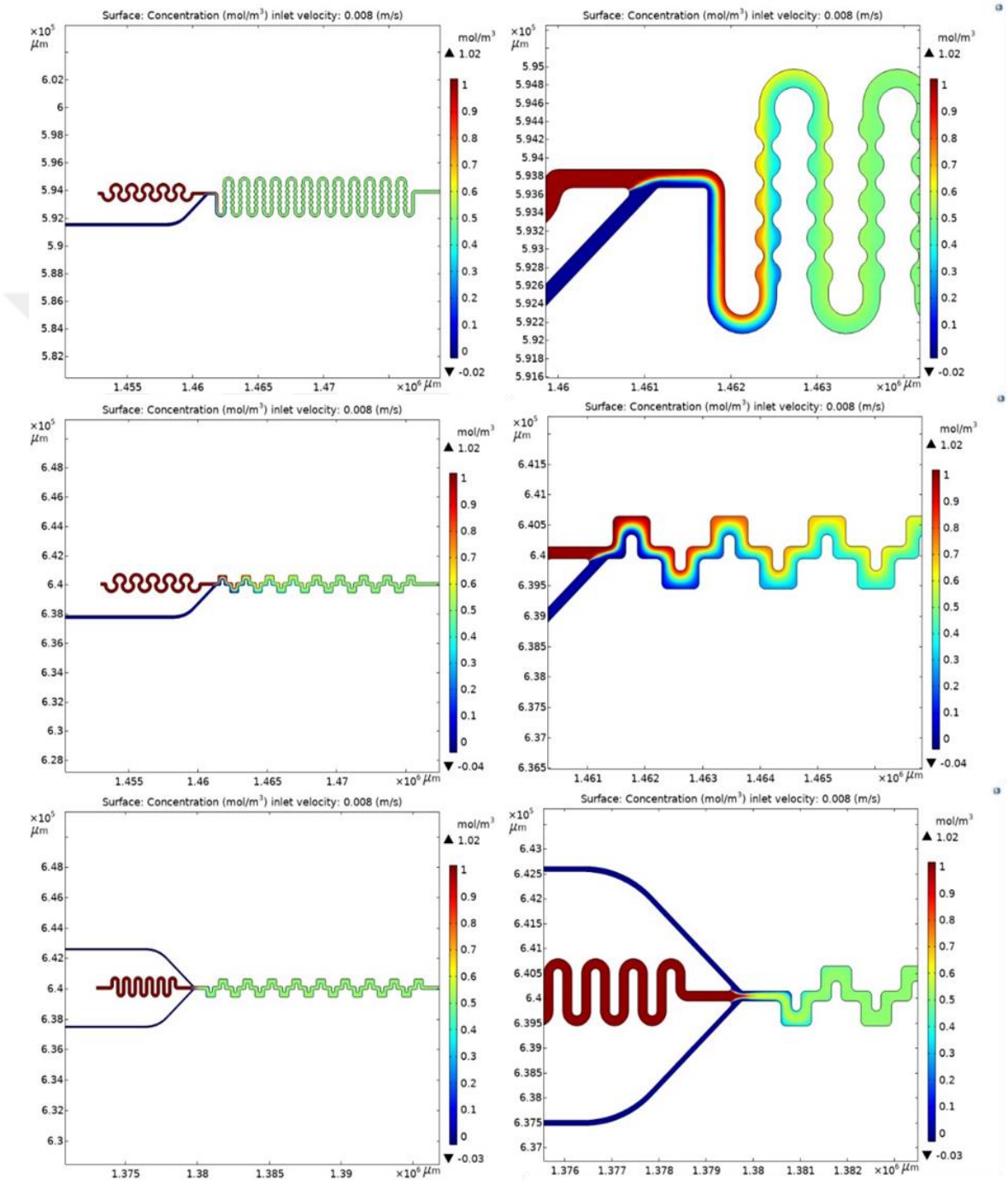

Figure 2.2 : Microfluidic channels flow simulation.

Reynolds number can be described as seen in equation 2.1:

$$RE = \frac{uL_C}{\nu} \tag{2.1}$$

Whereas, the Peclet number is calculated by solving equation 2.2:

$$Pe = \frac{uL_C}{D} \tag{2.2}$$

Where $\boldsymbol{u}$ is the velocity, $\boldsymbol{L_C}$ is the characteristic length of the flow, $\boldsymbol{\nu}$ is the kinematic viscosity of the fluid and $\boldsymbol{D}$ is the diffusion constant.

When water is the carrier fluid the relationship between the Reynolds number and Peclet number becomes as shown in equation 2.3:

$$Pe = 1000\ Re \tag{2.3}$$

The different flow rates and their corresponding Reynolds number and Peclet number for the designed micromixers are indicated in (Table 2.2) below.

Table 2.2 : Reynolds and Peclet numbers.

Inlet flow (mL/min)	Velocity(m/s)	Reynolds number (RE)	Peclet number (Pe)
0.005	0.00833	0.67	666.40
0.01	0.01666	1.33	1,332.80
0.015	0.025	2.00	2,000.00
0.02	0.033	2.64	2,640.00
0.025	0.0146	1.17	1,168.00
0.03	0.05	4.00	4,000.00
0.035	0.0583	4.66	4,664.00
0.04	0.0666	5.33	5,328.00
0.045	0.075	6.00	6,000.00
0.05	0.0833	6.66	6,664.00

3. DEVICE FABRICATION

In this chapter, the fabrication and assembly of the microfluidic channels are reported in detail.

3.1 Silicon Wafer Patterning

Microfluidic channel designs were patterned on 4-inch silicon wafers using photolithography. SUSS Microtec (MA6/BA6) machine was used to transfer the microfluidic geometries onto the silicon wafer through acetate masks. The microfluidic channels were designed using AutoCAD and saved as a GDSII file that was then sent to " Çözüm Tanıtım Hizmetleri Tic. Ltd. Şti." for acetate mask production.

Before any experimental steps, the silicon wafers were prepped to enhance the adhesion and uniformity of the coating photoresist. Isopropyl alcohol wash was used to remove dust or trace residues from the surface, then they were dried using a nitrogen gun and put on a hot plate at 200˚C for 1 minute to dehydrate the wafers.

The photoresist is a light-activated polymer used to transfer the pattern onto a substrate through a mask. When the photoresist is exposed to light, it can either become soluble or it can harden. When a positive photoresist is exposed through a patterned mask and developed it produces the same mask image on the surface of the substrate. However, when a negative photoresist is exposed and developed it produces a negative image of the mask. (Figure 3.1) shows the difference between a positive and a negative photoresist in microfabrication.

SU-8 3050 negative photoresist (MicroChem) is coated onto the silicon wafer using a Laurell WS-650MZ-23NPPB spin coating device to obtain a 50μm thickness on the substrates. After, the coated silicon wafer was transferred to a hotplate to prebake at 95˚C for 15 minutes to remove the residual solvent of the photoresist. The prebake helps in increasing coat stability, enhancing adhesion to the wafer, and removing any bubbles. The coated silicon wafer is then cooled down to room temperature before UV

exposure. SUSS Microtec (MA6/BA6) machine was used to expose the coated silicon wafer through the acetate photoresist.

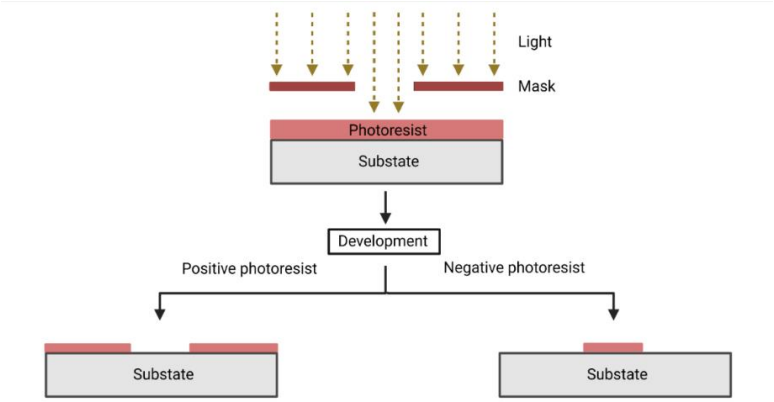

Figure 3.1 : Comparison between positive and negative photoresists.

Contact printing was used, where the acetate mask is placed directly on top of the coated wafer to obtain up to 1µm resolution. The pattern was transferred by exposure to a (260nm-325nm) light source for 10 seconds. Post-exposure bake (PEB) of the exposed wafer was carried out on a hotplate at 65˚C for 1 minute then at 95˚C for 5 minutes to provide any needed energy to continue the activation process of the exposed photoresist. To reveal the patterned design on the surface, the silicon wafer was submerged in a SU-8 developer bath and agitated for about 8 minutes until the 50µm high design is revealed. The patterned silicon wafer is then hard-baked on a hotplate at 150˚C for 20 minutes to increase its durability and remove any micro-cracks to produce the patterned silicon wafer as seen in (Figure 3.2). A summary of the fabrication steps and parameters can be seen in (Table 3.1).

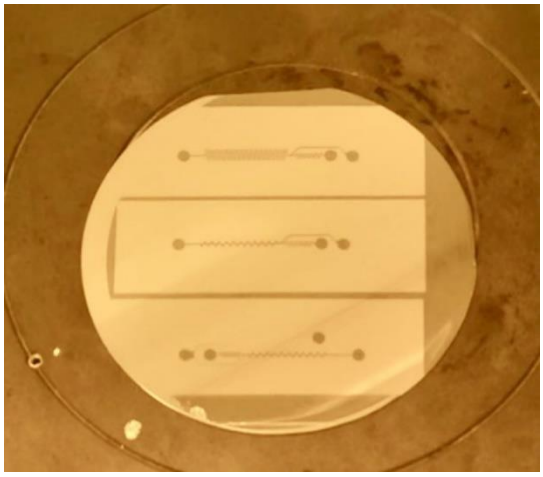

Figure 3.2 : Patterned silicon wafer**.**

Table 3.1 : Processes and parameters.

Process	Parameter
Spin Coat	500 Rpm - 5s , 3000 Rpm - 30s
Soft Bake	95˚C – 15min
Uv Exposure	250 Mj/Cm2 – 10s
Post Exposure Bake	65˚C – 1min, 95˚C – 5min
Development	SU8 developer – 8min
Hard Bake	150ºC – 20min

3.2 PDMS Microfluidic Channel

The patterned silicon wafer was used as the master mold to transfer the microfluidic channel geometry to PDMS, the replica molding process is demonstrated in (Figure 3.3).

PDMS was mixed with a hardening agent in a 10:1 ratio wt/wt and degassed using a desiccator for about 20 minutes. When all the bubbles are removed from the mixture, it is then poured onto the master mold and heated on a hotplate at 90˚C for 20 minutes, this allowed the solvent to evaporate and the PDMS to cure. After curing, the PDMS is peeled carefully from the master mold to punch in the inlets/outlets and cut the PDMS to fit on top of a glass slide. To bond the PDMS on the glass substrate oxygen plasma cleaner PDC-001 from “Harrick Plasma” to seal the bottom of the microfluidic channel. The cut PDMS sheets and glass substrates were first washed with isopropyl alcohol and dried using a nitrogen gun. Then, they were placed inside the Oxygen plasma cleaner chamber.

The chamber was vacuumed for 1.5 minutes before allowing oxygen in through the valve for 50 seconds. After sufficient oxygen was let in, the oxygen value was closed, and the machine was turned on and put on a high setting. When the plasma hue was observed, the PDMS and the glass substrates were exposed to the plasma for 50 seconds. Finally, the device was turned off and the samples were taken out and bonded immediately. Light tapping motion was applied to relieve any bubbles and ensure

complete contact between the surfaces. The fabricated microfluidic channels can be seen in (Figure 3.4).

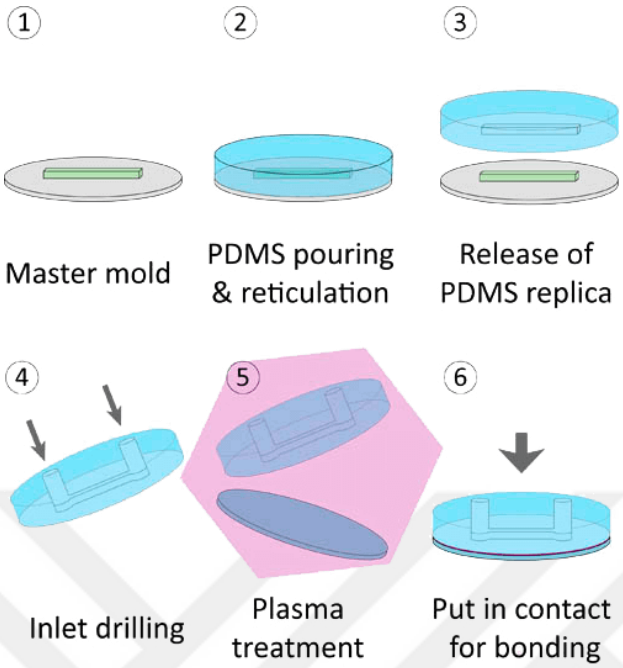

Figure 3.3 : Replica molding process [91].

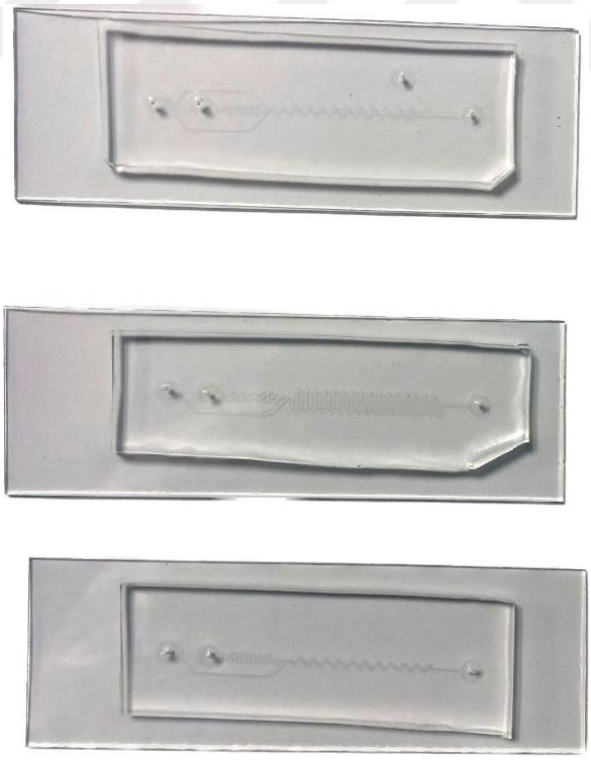

Figure 3.4 : The fabricated microfluidic systems.

3.3 Electrode Placement

DropSens DRP-GIDEAU10 gold interdigitated screen-printed electrodes (SPE) were purchased from “Metrohm”.

In order to create a well on the detection region of the screen-printed electrode, first a thin layer of PDMS was poured and cured on a clear smooth silicon wafer. The PDMS was then peeled and cut into two (55 mm x 27.5 mm) sheets. One of them was punched with a 5mm punch to create a hole that is aligned with the electrode’s detection region. A cutout with the same SPE dimensions is created on the second blank PDMS sheet and the first PDMS sheet is placed on top and the two PDMS sheets are bonded using the above-mentioned plasma bonding technique. The cutout. The SPE can be placed inside the cutout pocket and aligned the hole with the detection region as shown in (Figure 3.5).

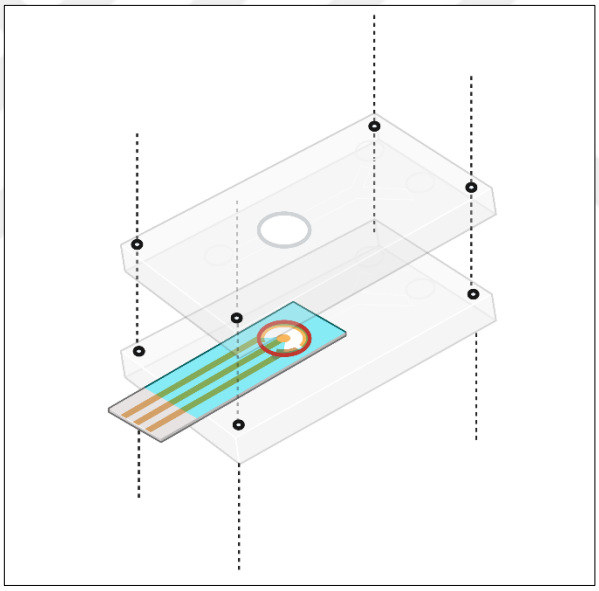

Figure 3.5 : Electrode alignment.

4. EXPERIMENTS AND RESULTS

4.1 Materials and Instruments

1 M, pH 7.4 Phosphate Buffer Solution from “Sigma-Aldrich”, DropSens DRP-GIDEAU10 gold interdigitated screen-printed electrodes (SPE) from “Metrohm”, Streptavidin-coated magnetic beads (Dynabeads™ M-280 Streptavidin) from “Thermofisher”, TWEEN 20 from “Merck”, Silicon tubes and connectors from “Nehir Biotechnology”, The peptide (SYVIH) was synthesized by TUBITAK and had a charge of +2, Syringe Pump PHD ULTRA from Harvard Apparatus and Agilent E4980A Precision LCR Meter.

4.2 Ink Test

The fabricated microfluidic channels were tested to verify their mixing efficiency in real-time. Two water-soluble dyes (red and blue) were diluted in distilled water, each dye was placed on an inlet using a micropipette tip. The flow of fluids inside the microfluidic channel was achieved by applying negative pressure on the outlet using a syringe pump. The dyes are infused through the microfluidic channel and mixed inside the micromixers. Good mixing is indicated by the formation of purple color at the microfluidic channel output. In (Figure 4.1), microscopic images of each microfluidic channel’s inlets and outlets are seen. The first microfluidic channel (the serpentine with constriction-expansion geometries) showed the best mixing results indicated by the purple color at the outlet. As for the second and third microfluidic channels, there’s still a distinction between the red and blue dye indicating sub-optimal mixing. The first microfluidic channel showed the best mixing owing to a longer mixing path and a larger number of constriction-expansion geometries that results in better mixing. Based on these results, the first microfluidic channel was chosen for further testing.

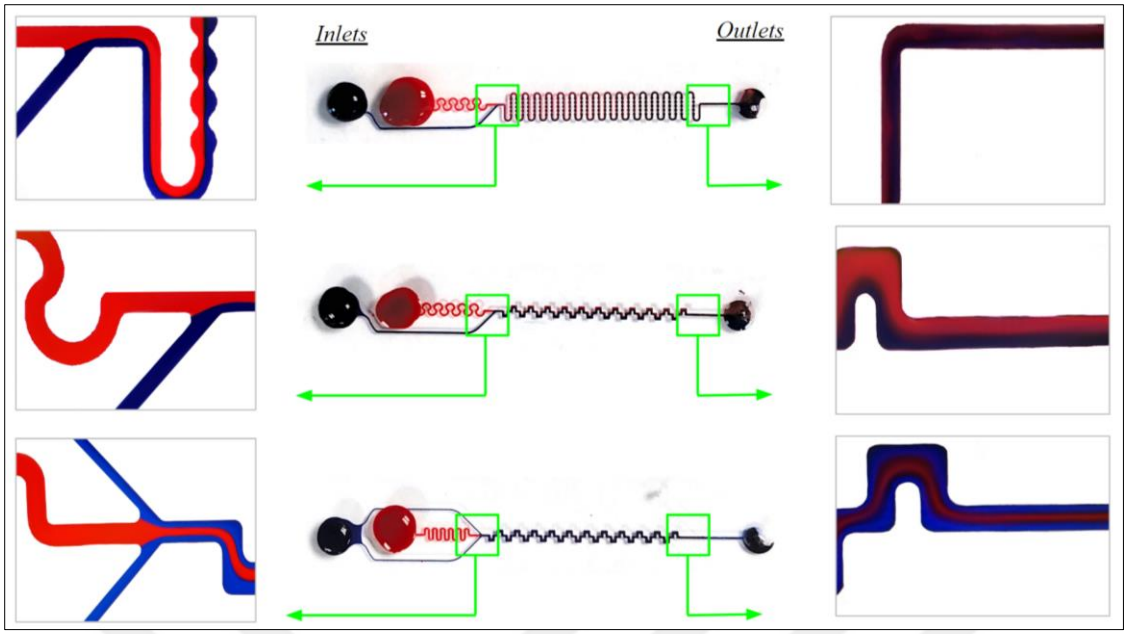

Figure 4.1 : Microscopic images of the inlets and outlets of the fabricated microfluidic channels.

4.3 Optimal PBS Concentration

Different molar concentrations of phosphate buffer solution (PBS) were prepared and their impedance signal was recorded. This process aims to determine the optimal PBS concentrations that would exhibit the highest impedance measurement over the tested frequency range.

0.001 mM, 0.01 mM, 0.1 mM, 1 mM, 10 mM, 50 mM, 100 mM, 500 mM, and 1 M of PBS solutions were prepared by diluting 1 M PBS with distilled water. The solutions were tested one by one by placing 100 µL of each solution on the SPE and recording the impedance measurements with Agilent Precision LCR Meter in a frequency range of (500 Hz- 250 kHz). 0.001 mM and 0.01 mM PBS measurements were neglected as they did not reproduce reliable impedance signals in the detection setup used. The magnitude of impedance was graphed against the frequency range to create a Bode plot as seen in (Figure 4.2). The impedance results show that as the ionic concentration of PBS increases the impedance decreases due to the increase in conductivity of the solution. Therefore, 0.1 mM of PBS was chosen as the optimal solution for electrochemical impedance spectroscopy due to its high impedance signal allowing for a higher impedance change in upcoming experiments.

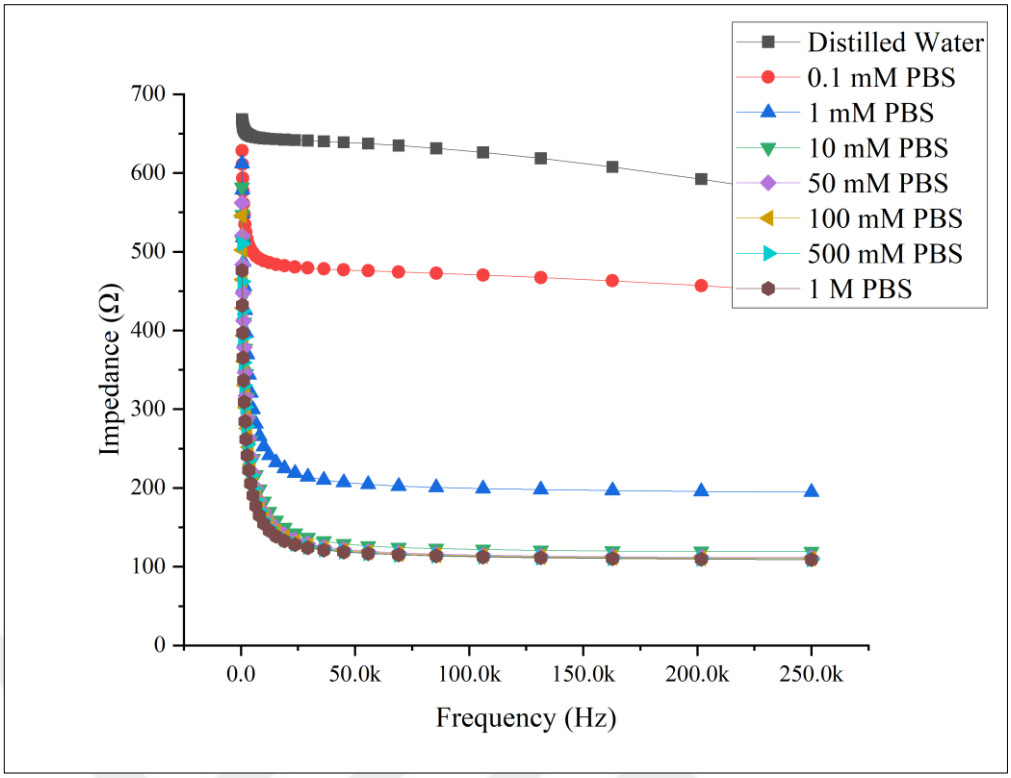

Figure 4.2 : Bode plot of different concentrations of PBS.

4.4 Impedance of Bare Magnetic Beads and Peptide Bound to Magnetic Beads

Generally, streptavidin-coated magnetic beads and biotinylated peptides are bounded through incubation to immobilize the biotinylated peptide on the surface of the magnetic beads. This procedure was carried out by TUBITAK to prepare samples and it followed the immobilization protocol mentioned in Dynabeads™ M-280 Streptavidin manual then the amount of bound peptide was quantified, and the steps are as follows:

1- The Dynabeads™ M-280 Streptavidin vial was agitated, and the desired volume of streptavidin-coated magnetic beads was taken, washed, and redispersed in the same volume of PBS.
2- The streptavidin-coated magnetic beads and the desired concentration of biotinylated peptide were incubated in PBS for 30 minutes with gentle mixing.
3- The peptide-bound magnetic beads were then separated using a magnet, and the supernatant with unbound biotinylated peptide was taken out. Then the sample was washed 3 times before resuspending in PBS.

4- BCA Protein Assay was used for colorimetric detection and quantitation of the amount of bound peptide to the magnetic beads and the concentrations of the bound peptide can be seen in (Table 4.1) below.

The impedance magnitude of these samples will be recorded later on.

Table 4.1 : Concentration of bound peptide in TUBITAK samples.

	The concentrations of bound peptide
Sample 1	0.0144 mg/mL
Sample 2	0.0341 mg/mL
Sample 3	0.0568 mg/mL
Sample 4	0.0578 mg/mL

To record the impedance of streptavidin-coated magnetic beads alone, 4 samples of 0.1 mg bare magnetic beads were prepared and their impedance measurements were recorded. 10 μL of 10 mg/mL streptavidin-coated magnetic beads were placed in a microtube with 40 μL of 0.1 mM PBS to wash the magnetic beads. The solution was vortexed for a few seconds before immobilizing the magnetic beads on the wall of the microtube with an external magnet. The supernatant was disposed and the clean magnetic beads were redispersed in 100 μL of 0.1 mM PBS. The prepared solution was placed on the SPE and it contained 0.1 mg of magnetic beads, which were immobilized on the surface of the SPE by placing a magnet under the detection zone. The impedance measurements were taken 1-2 minutes after the placement of the solution to allow the magnetic beads to immobilize on the surface of SPE and the same frequency range of (500 Hz- 250 kHz) was used. The same process was repeated for all 4 samples. The average impedance of the 4 samples and The impedance of 0.1mM PBS were graphed in (Figure 4.3), where the addition of magnetic beads to the solutions reduces the impedance magnitude due to the conductive nature of the beads.

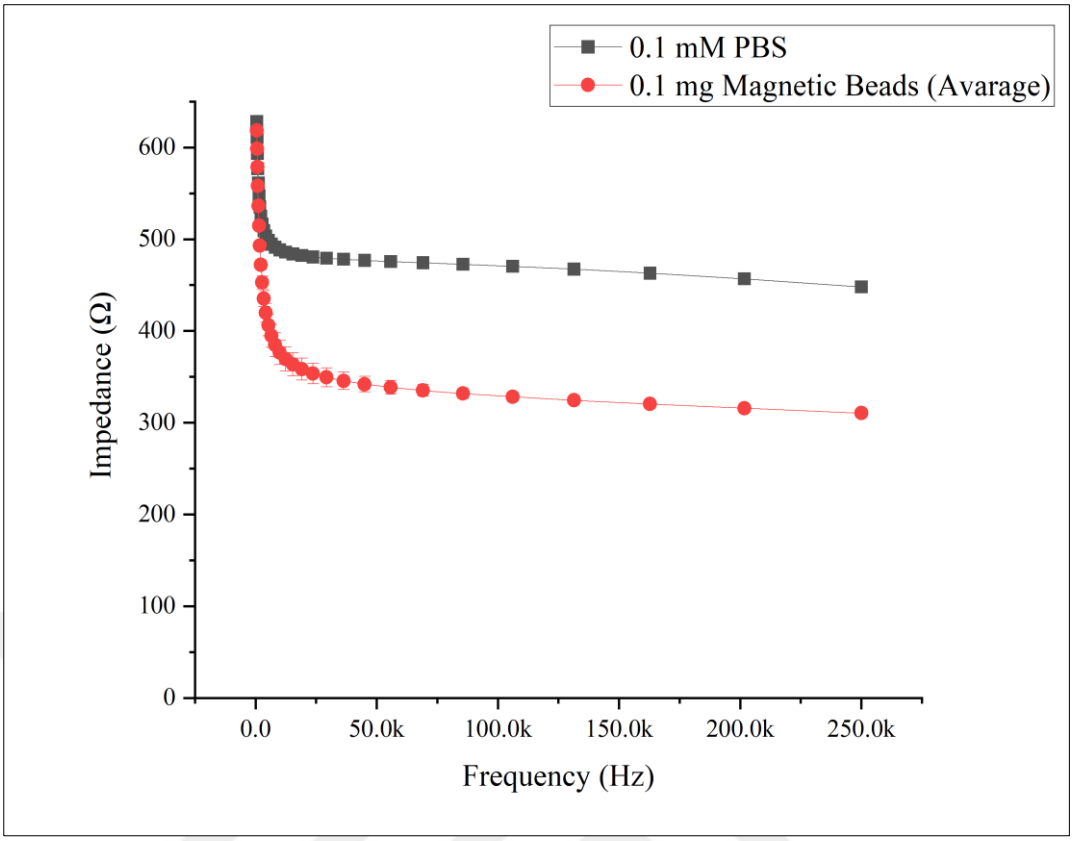

Figure 4.3 : Bode plot of 0.1 mM PBS and 0.1 mM PBS with 0.1 mg magnetic beads.

Then biotinylated peptide bound to streptavidin-coated magnetic beads were washed as previously described above and resuspended in 100 µL 0.1 mM PBS for impedance measurements. Each sample was immobilized on the surface of the SPE with an external magnet and its impedance was recorded. This process aims to measure the impedance change as the amount of bound peptide is increased and to obtain a calibration curve to determine the amount of bound peptide in further experiments. The highest correlation coefficient (0.984659) was recorded at a frequency of 12.4 kHz. The impedance magnitude of these samples is shown in (Figure 4.4). The Bode plot demonstrates the reduction in measured impedance as the concentration of the bound peptide increases. This is owed to the peptide charge of +2 that facilitates charge transfer at the surface of the SPE.

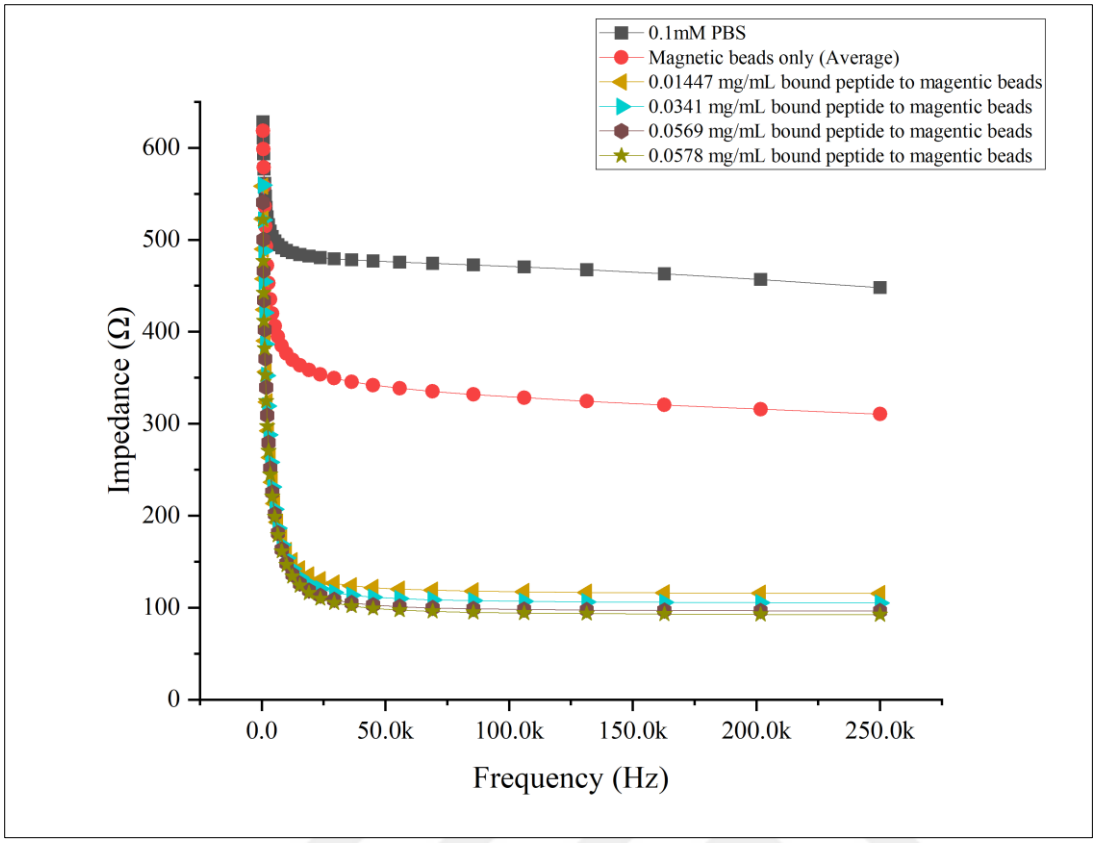

Figure 4.4 : Bode plot of peptide bound to magnetic beads.

4.5 Impedance of Free Peptide

3 different concentrations (0.2, 0.3, 0.4 mg/mL) of free peptide were prepared in 100 µL 0.1 mM PBS. These measurements were taken to validate the decrease in impedance magnitude in relation to the increased concentration of peptide. The measurements were repeated 3 times to validate the results and the average of their impedance is graphed in (Figure 4.5) along with the impedance magnitude of 0.1 mM PBS, the average of bare magnetic beads, and TUBITAK samples. The impedance of free peptide has a higher magnitude than TUBITAK samples owing to the absence of magnetic beads that increase the conductance when present.

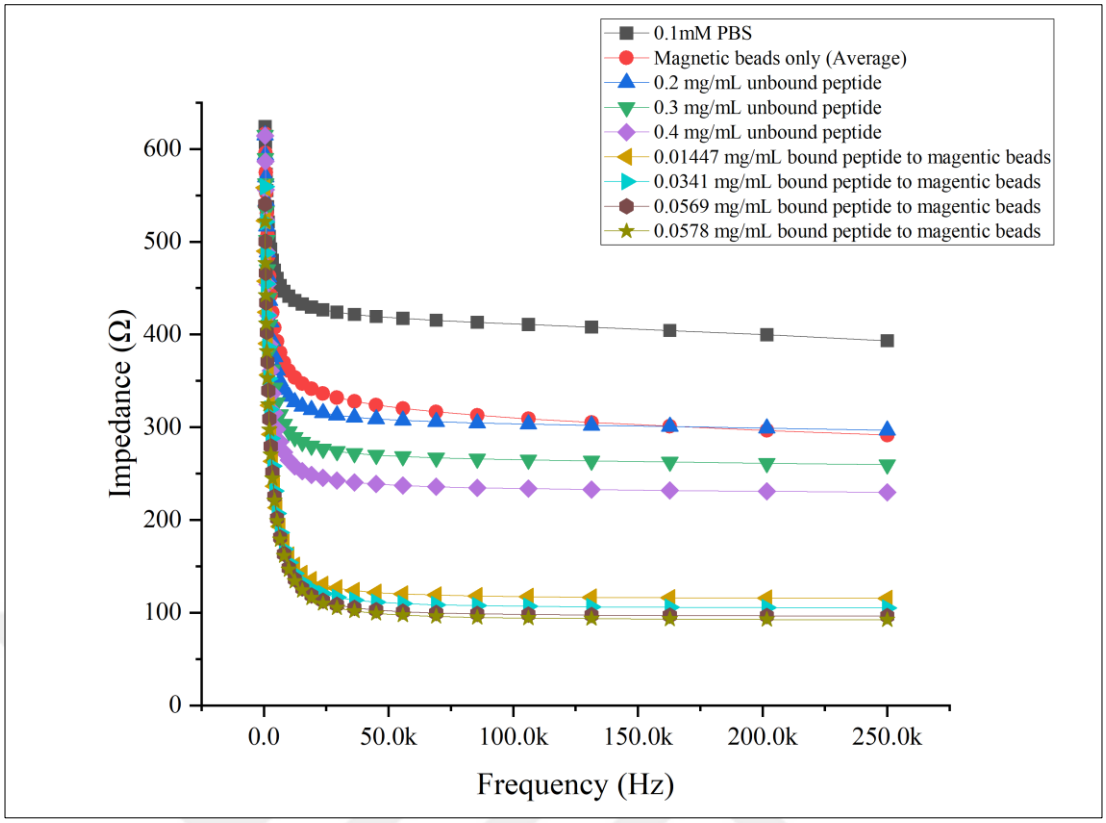

Figure 4.5 : Bode plot of 0.1 mM, bare magnetic beads, free peptide, and TUBITAK samples.

4.6 Increasing The Hydrophilicity of Microfluidic Channel

PDMS is a hydrophobic material resulting in the adsorption of hydrophobic analytes on the microfluidic channel walls. To inhibit the adsorption of Dynabeads™ M-280 Streptavidin which are characterized as hydrophobic beads and the adsorption of peptides, the use of surfactant is recommended. Tween 20 (Polysorbate 20) is a non-ionic surfactant that is widely used due to its nontoxicity and compatibility in biological applications. Free magnetic beads were infused in the same channel before and after surfactant treatment to compare its effect.

First 0.1 mg of free magnetic beads were washed and suspended into 600 µL 0.1 mM PBS, and 300 µL were infused from each inlet at a flow rate of 50 µL/min. After the infusion of the sample, the microfluidic channel was flushed with 200 µL of 0.1mM PBS The output was collected from the outlet in a microtube and a strong neodymium magnet was fixed on the wall of the microtube to collect the magnetic beads. No magnetic beads were collected on the microtube's wall indicating that a significant amount of magnetic beads were lost and therefore, no impedance measurement was

recorded. The microfluidic channel was inspected under the microscope to confirm the presence of the magnetic beads in the micromixer. (Figure 4.6 a) illustrates the presence of the infused magnetic beads on the channel walls.

0.3% v/v Tween 20 solution was prepared using 0.1mM PBS. 1 mL of the surfactant solution was infused through the microfluidic channel at a flow rate of 50 µL/min. After the infusion of the surfactant solution, the channel was flushed with 1 mL of 0.1 mM PBS at the same flow rate. After treating the microfluidic channel with the surfactant, the experiment was repeated with the same amount of magnetic beads, volumes, and flow rate. When the magnet was placed on the side of the microtube, the magnetic beads started collecting immediately. While the magnetic beads were immobilized by the magnet, the solution was disposed of, and 100 µL of 0.1 mM PBS was added. The sample was vortexed and impedance measurement was recorded. (Figure 4.7) shows the impedance magnitude of the reference 0.1 mg magnetic beads and the recovered beads from the microfluidic channel after the treatment with Tween 20. (Figure 4.6 b) shows the micromixer walls after the surfactant treatment.

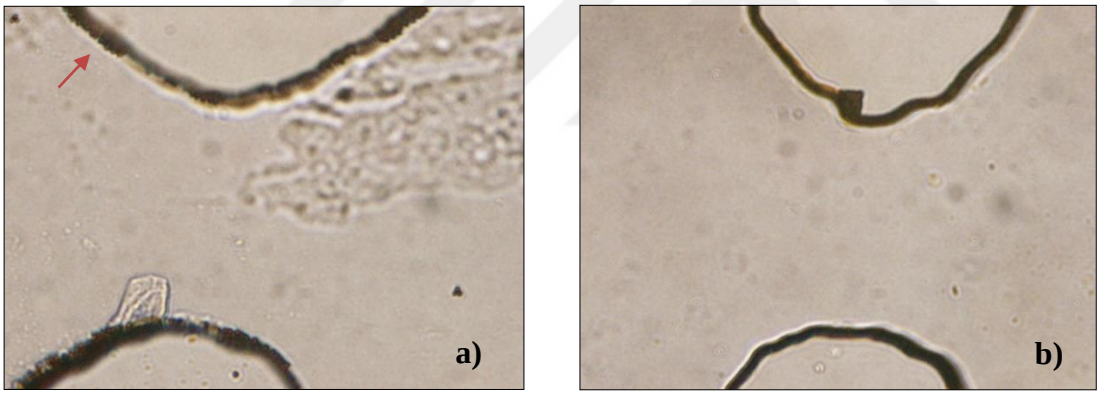

Figure 4.6 : Microfluidic channel walls (a) before 0.3% Tween 20 (b) after 0.3% Tween 20.

The impedance magnitude of the recovered beads shows the successful recovery of magnetic beads after treating the microfluidic channel with 0.3% Tween 20. The increase in impedance magnitude can be attributed to the binding of Tween 20 hydrophobically to the streptavidin-coated magnetic beads educing its conductance.

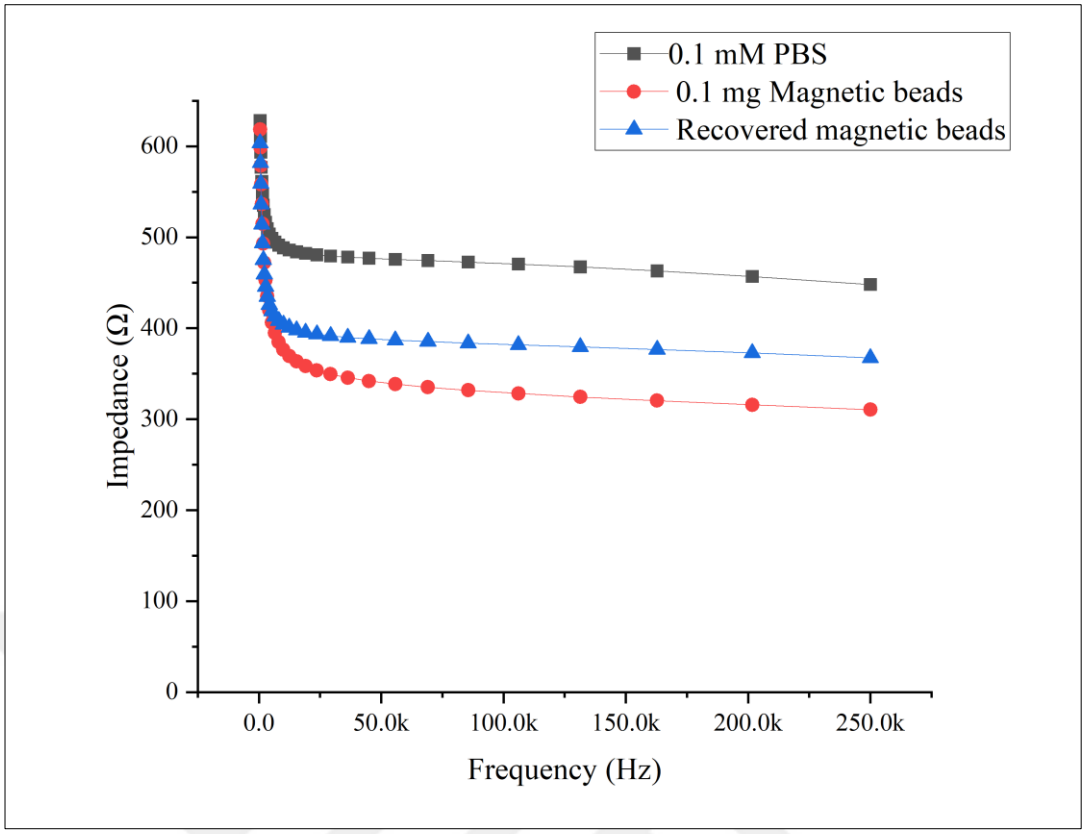

Figure 4.7 : Recovery of magnetic beads from the microfluidic channel.

4.7 The Microfluidic Channel

Two different concentrations of biotinylated peptide (50, and 200) µg/mL were infused through the microfluidic channel with 0.1 mg of streptavidin-coated magnetic beads. Biotinylated peptide and streptavidin-coated magnetic beads were infused from separate inlets as seen in (Figure 4.8) at two different flow rates 10 µL/min and 50 µL/min. The amount of infused species and their flow rates are shown in (Table 4.2).

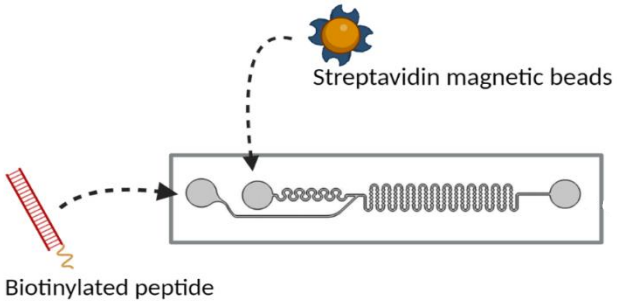

Figure 4.8 : Schematic representation of infused species.

Table 4.2 : The amount of infused species and their flow rates.

Streptavidin magnetic beads (mg)	Biotinylated peptide (µg/mL)	Flow rate (µL/min)
0.1	50	10
0.1	200	10
0.1	50	50
0.1	200	50

Each sample was prepared in 300 µL of 0.1 mM PBS and infused through the microfluidic channel from different inlets for a total infusion volume of 600 µL for streptavidin magnetic beads and biotinylated peptide. After each sample infusion, the microfluidic channel was flushed with 200 µL of 0.1 mM PBS infused from both inlets. The output is collected in a microtube and the magnetic beads were separated for impedance measurements, The process of output sample collection and measurement is demonstrated in (Figure 4.9). The output solution should contain unbound peptides, unbound streptavidin-coated magnetic beads, and peptide bound to magnetic beads. An external magnet is used to separate the magnetic beads (bound and unbound) from the supernatant solution before discarding it and adding 100 µL of 0.1 mM PBS for subsequent impedance measurements.

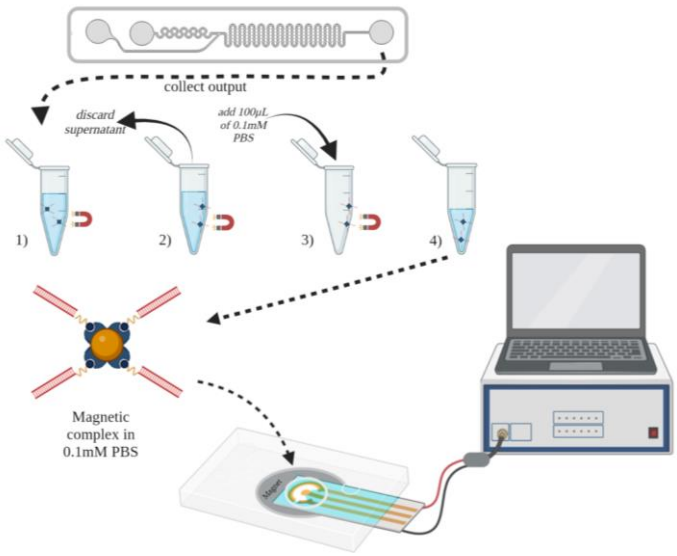

Figure 4.9 : Process of magnetic beads extraction and measurement.

The impedance magnitude of the collected magnetic beads from the output of the microfluidic channel is shown in (Figure 4.10). All the samples had an impedance magnitude close to the impedance magnitude of the recovered unbound magnetic beads indicating that there was only a tiny amount of peptide binding on magnetic beads or no binding at all during infusion. The limited interaction between streptavidin-coated magnetic beads and biotinylated peptide could be due to the limited incubation time and the constant rotation of the streptavidin-coated magnetic beads which limits the interaction between streptavidin and biotin. Additionally, the increase in the impedance magnitude could be due to the interaction between the infused sample and Tween 20, which can reduce the conductance of the samples and could hinder the interaction between the biotinylated peptide and the streptavidin-coated magnetic beads. Further investigation is needed to verify whether there was any binding between infused species.

These experiments are part of an ongoing TUBITAK project to develop a microfluidic immunosensor for the early detection of liver cancer. Further experiments will be conducted with Alpha Fetoprotein antigen and antibody to fine-tune the experimental setup to achieve a sensitive microfluidic immunosensor.

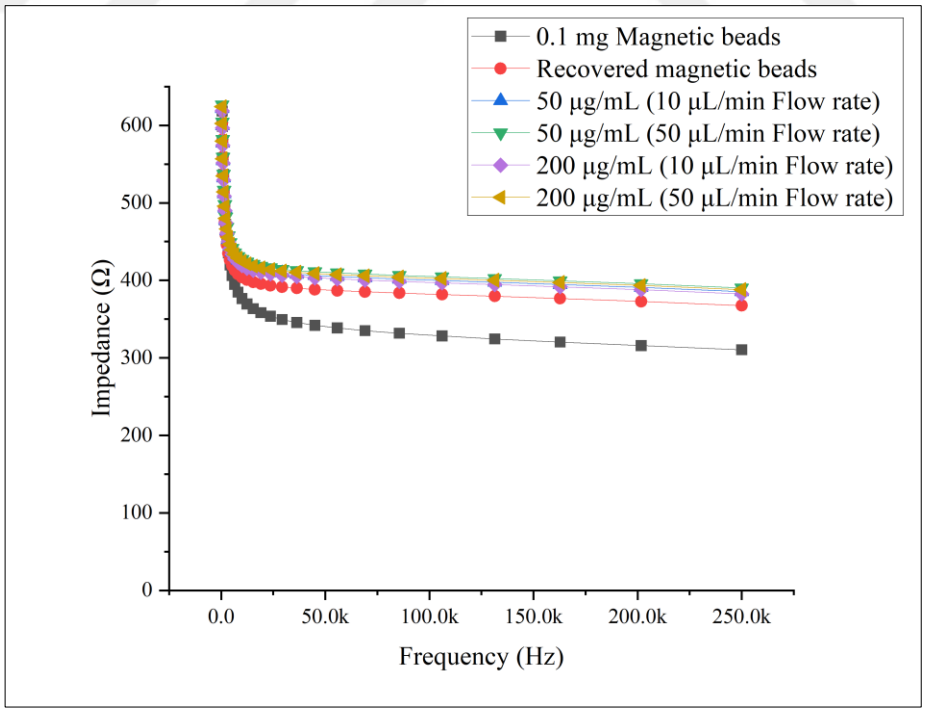

Figure 4.10 : Impedance magnitude of the microfluidic channel output.

5. CONCLUSION AND RECOMMENTATIONS

In this study, the successful fabrication of microfluidic micromixers was reported. Three micromixers were designed to adapt constriction-expansion geometries and asymmetric square wave geometries to induce turbulence in the fluid flow. All three geometries were simulated using COMSOL Multiphysics software to visualize the mixing of two fluids inside the microfluidic channel and results showed that effective mixing was achieved. Microfabrication techniques such as photolithography and soft lithography were utilized to fabricate the silicon master mold and the microfluidic channels successfully. Electrochemical impedance spectroscopy was used to analyze streptavidin-coated magnetic beads and biotinylated peptides and the samples infused through the channel. 0.1 mM PBS was chosen as the solution for impedance measurements as it illustrated the highest impedance signal of all PBS solutions which would result in the highest impedance change when the impedance of streptavidin-coated magnetic beads and biotinylated peptide is recorded. EIS results showed that the increased binding of the biotinylated peptide to the streptavidin-coated magnetic beads reduces the impedance signal due to the charge of the peptide. The microfluidic channel was successfully coated with 0.3% Tween 20 in 0.1 mM PBS which aids in the recovery of magnetic beads from the microfluidic channel and reduces the desorption of magnetic beads and peptide on the microfluidic channel walls. Evidence of peptide binding on magnetic beads is not clear. This could be a result of low incubation time or due to the coating of Tween 20 on the surface of the infused samples. These reasons can result in suboptimum binding since mixing is proven to be efficient. Further comprehensive tests are needed to verify the presence or absence of bound peptides on the surface of magnetic beads.

This work was supported by TUBITAK under project No. 20AG012.

REFERENCES

[1] **Schrittwieser, S., Pelaz, B., Parak, W. J., Lentijo-Mozo, S., Soulantica, K., Dieckhoff, J., Ludwig, F., Guenther, A., Tschöpe, A., & Schotter, J.** (2016). Homogeneous Biosensing Based on Magnetic Particle Labels. *Sensors (Basel, Switzerland)*, *16*(6), 828. https://doi.org/10.3390/s16060828

[2] **Kumar, S., Kumar, S., Ali, Md. A., Anand, P., Agrawal, V. V., John, R., Maji, S., & Malhotra, B. D.** (2013). Microfluidic-integrated biosensors: Prospects for point-of-care diagnostics. *Biotechnology Journal*, *8*(11), 1267–1279. https://doi.org/10.1002/biot.201200386

[3] **Henares, T. G., Mizutani, F., & Hisamoto, H.** (2008). Current development in microfluidic immunosensing chip. *Analytica Chimica Acta*, *611*(1), 17–30. https://doi.org/10.1016/j.aca.2008.01.064

[4] **Chircov, C., Bîrcă, A. C., Grumezescu, A. M., & Andronescu, E.** (2020). Biosensors-on-Chip: An Up-to-Date Review. *Molecules*, *25*(24), Article 24. https://doi.org/10.3390/molecules25246013

[5] **Lynn, N. S.** (2018). Microfluidic Mixing for Biosensors. In S.-H. Oh, C. Escobedo, & A. G. Brolo (Eds.), *Miniature Fluidic Devices for Rapid Biological Detection* (pp. 69–103). Springer International Publishing. https://doi.org/10.1007/978-3-319-64747-0_3

[6] **Lee, C.-Y., Wang, W.-T., Liu, C.-C., & Fu, L.-M.** (2016). Passive mixers in microfluidic systems: A review. *Chemical Engineering Journal*, *288*, 146–160. https://doi.org/10.1016/j.cej.2015.10.122

[7] **Echouchene, F., Al-shahrani, T., & Belmabrouk, H.** (2021). Enhancement of Heterogeneous Microfluidic Immunosensors Using New Sensing Area Shape with Electrothermal Effect. *Applied Sciences*, *11*(10), Article 10. https://doi.org/10.3390/app11104566

[8] **Verma, S., & Panda, S.** (2021). Study of capture efficiency utilizing passive mixing in heterogeneous microfluidic immunosensors. *Chemical Engineering and Processing - Process Intensification*, 108708. https://doi.org/10.1016/j.cep.2021.108708

[9] **Yang, K., Islam, N., Eda, S., & Wu, J.** (2017). Optimization of an AC electrokinetics immunoassay lab-chip for biomedical diagnostics. *Microfluidics and Nanofluidics*, *21*(3), 35. https://doi.org/10.1007/s10404-017-1867-x

[10] **Hart, R., Lec, R., & Noh, H. "Moses."** (2010). Enhancement of heterogeneous immunoassays using AC electroosmosis. *Sensors and Actuators B: Chemical*, *147*(1), 366–375. https://doi.org/10.1016/j.snb.2010.02.027

[11] **Sigurdson, M., Wang, D., & D. Meinhart, C.** (2005). Electrothermal stirring for heterogeneous immunoassays. *Lab on a Chip*, *5*(12), 1366–1373. https://doi.org/10.1039/B508224B

[12] **Selmi, M., Khemiri, R., Echouchene, F., & Belmabrouk, H.** (2016). Enhancement of the Analyte Mass Transport in a Microfluidic Biosensor by Deformation of Fluid Flow and Electrothermal Force. *Journal of Manufacturing Science and Engineering*, *138*(8). https://doi.org/10.1115/1.4033484

[13] **Selmi, M., Gazzah, M. H., & Belmabrouk, H.** (2017). Optimization of microfluidic biosensor efficiency by means of fluid flow engineering. *Scientific Reports*, *7*(1), Article 1. https://doi.org/10.1038/s41598-017-06204-0

[14] **Selmi, M., Echouchene, F., Gazzah, M. H., & Belmabrouk, H.** (2015). Flow Confinement Enhancement of Heterogeneous Immunoassays in Microfluidics. *IEEE Sensors Journal*, *15*(12), 7321–7328. https://doi.org/10.1109/JSEN.2015.2475610

[15] **Lee, H. J., Lee, S. H., Yasukawa, T., Ramón-Azcón, J., Mizutani, F., Ino, K., Shiku, H., & Matsue, T.** (2010). Rapid and simple immunosensing system for simultaneous detection of tumor markers based on negative-dielectrophoretic manipulation of microparticles. *Talanta*, *81*(1–2), 657–663. https://doi.org/10.1016/j.talanta.2009.12.058

[16] **C. Feldman, H., Sigurdson, M., & D. Meinhart, C.** (2007). AC electrothermal enhancement of heterogeneous assays in microfluidics. *Lab on a Chip*, *7*(11), 1553–1559. https://doi.org/10.1039/B706745C

[17] **Porter, J. M., Modares, P., Castiello, F. R., & Tabrizian, M.** (2019). Capacitive Detection of Insulin Antibody enhanced by AC Electrothermal mixing. *2019 IEEE 6th Portuguese Meeting on Bioengineering (ENBENG)*, 1–4. https://doi.org/10.1109/ENBENG.2019.8692504

[18] **Salari, A., & Thompson, M.** (2018). Recent advances in AC electrokinetic sample enrichment techniques for biosensor development. *Sensors and Actuators B: Chemical*, *255*, 3601–3615. https://doi.org/10.1016/j.snb.2017.09.069

[19] **Koklu, A., Giuliani, J., Monton, C., & Beskok, A.** (2020). Rapid and Sensitive Detection of Nanomolecules by an AC Electrothermal Flow Facilitated Impedance Immunosensor. *Analytical Chemistry*, *92*(11), 7762–7769. https://doi.org/10.1021/acs.analchem.0c00890

[20] **Huang, Y., Sun, T., Liu, L., Xia, N., Zhao, Y., & Yi, X.** (2021). Surface plasmon resonance biosensor for the detection of miRNAs by combining the advantages of homogeneous reaction and heterogeneous detection. *Talanta*, *234*, 122622. https://doi.org/10.1016/j.talanta.2021.122622

[21] **Cristea, C., Florea, A., Tertis, M., & Sandulescu, R.** (2015). Immunosensors. In T. Rinken (Ed.), *Biosensors—Micro and Nanoscale Applications*. InTech. https://doi.org/10.5772/60524

[22] **Bange, A., Halsall, H. B., & Heineman, W. R.** (2005). Microfluidic immunosensor systems. *Biosensors and Bioelectronics*, *20*(12), 2488–2503. https://doi.org/10.1016/j.bios.2004.10.016

[23] **Kundu, P. K., Cohen, I. M., & Dowling, D. R.** (2016). Chapter 9—Laminar Flow. In P. K. Kundu, I. M. Cohen, & D. R. Dowling (Eds.), *Fluid Mechanics (Sixth Edition)* (pp. 409–467). Academic Press. https://doi.org/10.1016/B978-0-12-405935-1.00009-5

[24] **Bayareh, M., Ashani, M. N., & Usefian, A.** (2020). Active and passive micromixers: A comprehensive review. *Chemical Engineering and Processing - Process Intensification*, *147*, 107771. https://doi.org/10.1016/j.cep.2019.107771

[25] **Lee, C.-Y., Chang, C.-L., Wang, Y.-N., & Fu, L.-M.** (2011). Microfluidic Mixing: A Review. *International Journal of Molecular Sciences*, *12*(5), 3263–3287. https://doi.org/10.3390/ijms12053263

[26] **Ward, K., & Fan, Z. H.** (2015). Mixing in microfluidic devices and enhancement methods. *Journal of Micromechanics and Microengineering*, *25*(9), 094001. https://doi.org/10.1088/0960-1317/25/9/094001

[27] **Yang, A.-S., Chuang, F.-C., Chen, C.-K., Lee, M.-H., Chen, S.-W., Su, T.-L., & Yang, Y.-C.** (2015). A high-performance micromixer using three-dimensional Tesla structures for bio-applications. *Chemical Engineering Journal*, *263*, 444–451. https://doi.org/10.1016/j.cej.2014.11.034

[28] **Gao, R., Lv, Z., Mao, Y., Yu, L., Bi, X., Xu, S., Cui, J., & Wu, Y.** (2019). SERS-Based Pump-Free Microfluidic Chip for Highly Sensitive Immunoassay of Prostate-Specific Antigen Biomarkers. *ACS Sensors*, *4*(4), 938–943. https://doi.org/10.1021/acssensors.9b00039

[29] **Guo, L., Shi, Y., Liu, X., Han, Z., Zhao, Z., Chen, Y., Xie, W., & Li, X.** (2018). Enhanced fluorescence detection of proteins using ZnO nanowires integrated inside microfluidic chips. *Biosensors and Bioelectronics*, *99*, 368–374. https://doi.org/10.1016/j.bios.2017.08.003

[30] **Zhan, Z., Yao, P., Dong, Z., Tung, S., Hohnbaum, J., Srinivasan, B., & Li, W. J.** (2010). Insulin detection based on a PDMS microfluidic system. *2010 IEEE International Conference on Nano/Molecular Medicine and Engineering*, 112–116. https://doi.org/10.1109/NANOMED.2010.5749815

[31] **Zheng, Z., Wu, L., Li, L., Zong, S., Wang, Z., & Cui, Y.** (2018). Simultaneous and highly sensitive detection of multiple breast cancer biomarkers in real samples using a SERS microfluidic chip. *Talanta*, *188*, 507–515. https://doi.org/10.1016/j.talanta.2018.06.013

[32] **Yin, B.-F., Wan, X.-H., Yang, M.-Z., Qian, C.-C., & Sohan, A. S. M. M. F.** (2022). Wave-shaped microfluidic chip assisted point-of-care testing for accurate and rapid diagnosis of infections. *Military Medical Research*, *9*(1), 8. https://doi.org/10.1186/s40779-022-00368-1

[33] **Sun, S., Luo, J., Zhu, Y., Kong, F., Mao, G., Ming, T., Xing, Y., Liu, J., Dai, Y., Yan, S., Yang, Y., & Cai, X.** (2022). Multifunctional self-driven origami paper-based integrated microfluidic chip to detect CRP and PAB in whole blood. *Biosensors and Bioelectronics*, *208*, 114225. https://doi.org/10.1016/j.bios.2022.114225

[34] **Vasantham, S., Alhans, R., Singhal, C., Nagabooshanam, S., Nissar, S., Basu, T., Ray, S. C., Wadhwa, S., Narang, J., & Mathur, A.** (2019). Paper based point of care immunosensor for the impedimetric detection of cardiac troponin I biomarker. *Biomedical Microdevices*, *22*(1), 6. https://doi.org/10.1007/s10544-019-0463-0

[35] **Ortega, F. G., Gómez, G. E., González-Martinez, C., Valero, T., Expósito-Hernández, J., Puche, I., Rodriguez-Martinez, A., Serrano, M. J., Lorente, J. A., & Fernández-Baldo, M. A.** (2022). A Novel, Quick, and Reliable Smartphone-Based Method for Serum PSA Quantification: Original Design of a Portable Microfluidic Immunosensor-Based System. *Cancers*, *14*(18), Article 18. https://doi.org/10.3390/cancers14184483

[36] **de Oliveira, T. R., Erbereli, C. R., Manzine, P. R., Magalhães, T. N. C., Balthazar, M. L. F., Cominetti, M. R., & Faria, R. C.** (2020). Early Diagnosis of Alzheimer's Disease in Blood Using a Disposable Electrochemical Microfluidic Platform. *ACS Sensors*, *5*(4), 1010–1019. https://doi.org/10.1021/acssensors.9b02463

[37] **Piguillem, S. V., Regiart, M., Bertotti, M., Raba, J., Messina, G. A., & Fernández-Baldo, M. A.** (2020). Microfluidic fluorescence immunosensor using ZnONFs for invasive aspergillosis determination. *Microchemical Journal*, *159*, 105371. https://doi.org/10.1016/j.microc.2020.105371

[38] **Nguyen, N.-T.** (2012). *Micromixers: Fundamentals, design, and fabrication* (2nd ed). Elsevier/William Andrew.

[39] **Leamon, J.** (2007). Cramming more sequencing reactions onto microreactor chips. *Chemical Reviews*. https://www.academia.edu/61731788/Cramming_more_sequencing_reactions_onto_microreactor_chips

[40] **Cai, G., Xue, L., Zhang, H., & Lin, J.** (2017). A Review on Micromixers. *Micromachines*, *8*(9), 274. https://doi.org/10.3390/mi8090274

[41] **Mensing, G. A., Pearce, T. M., Graham, M. D., & Beebe, D. J.** (2004). An externally driven magnetic microstirrer. *Philosophical Transactions. Series A, Mathematical, Physical, and Engineering Sciences*, *362*(1818), 1059–1068. https://doi.org/10.1098/rsta.2003.1362

[42] **Gambhire, S., Patel, N., Gambhire, G., & Kale, S.** (2011). A Review on Different Micromixers and its Micromixing within Microchannel. *International Journal of Current Engineering and Technology*. https://doi.org/10.14741/Ijcet/22774106/spl.4.2016.83

[43] **Stroock, A. D., Dertinger, S. K. W., Ajdari, A., Mezić, I., Stone, H. A., & Whitesides, G. M.** (2002). Chaotic Mixer for Microchannels. *Science*, *295*(5555), 647–651. https://doi.org/10.1126/science.1066238

[44] **Hessel, V., Hardt, S., Löwe, H., & Schönfeld, F.** (2003). Laminar mixing in different interdigital micromixers: I. Experimental characterization. *AIChE Journal*, *49*(3), 566–577. https://doi.org/10.1002/aic.690490304

[45] **Udaya Kumar, A., Sai Ganesh, D., Vamsi Krishna, T., Sashank, B., & Satyanarayana, T.** (2022). Modeling and investigation on mixing characteristics of T & Y-shaped micromixers for microfluidic devices. *Materials Today: Proceedings*, *59*, 501–505. https://doi.org/10.1016/j.matpr.2021.11.474

[46] **Tofteberg, T., Skolimowski, M., Andreassen, E., & Geschke, O.** (2010). A novel passive micromixer: Lamination in a planar channel system. *Microfluidics and Nanofluidics*, *8*(2), 209–215. https://doi.org/10.1007/s10404-009-0456-z

[47] **Wong, S. H., Ward, M. C. L., & Wharton, C. W.** (2004). Micro T-mixer as a rapid mixing micromixer. *Sensors and Actuators B: Chemical*, *100*(3), 359–379. https://doi.org/10.1016/j.snb.2004.02.008

[48] **Url-1** <https://link.springer.com/article/10.1007/s10404-006-0079-6>, date retrieved 15.10.2022.

[49] **Jiang, F., Drese, K., Hardt, S., Küpper, M., & Schönfeld, F.** (2004). Helical Flows and Chaotic Mixing in Curved Microchannels. *AIChE Journal*, *50*, 2297–2305. https://doi.org/10.1002/aic.10188

[50] **Mengeaud, V., Josserand, J., & Girault, H. H.** (2002). Mixing Processes in a Zigzag Microchannel: Finite Element Simulations and Optical Study. *Analytical Chemistry*, *74*(16), 4279–4286. https://doi.org/10.1021/ac025642e

[51] **Liu, R. H., Stremler, M. A., Sharp, K. V., Olsen, M. G., Santiago, J. G., Adrian, R. J., Aref, H., & Beebe, D. J.** (2000). Passive mixing in a three-dimensional serpentine microchannel. *Journal of Microelectromechanical Systems*, *9*(2), 190–197. https://doi.org/10.1109/84.846699

[52] **Vijayendran, R., Motsegood, K., Beebe, D., & Leckband, D.** (2003). Evaluation of a Three-Dimensional Micromixer in a Surface-Based Biosensor†. *Langmuir*, *19*, 1824–1828. https://doi.org/10.1021/la0262250

[53] **Kim, D. S., Lee, S. H., Kwon, T. H., & Ahn, C. H.** (2005). A serpentine laminating micromixer combining splitting/recombination and advection. *Lab on a Chip*, *5*(7), 739. https://doi.org/10.1039/b418314b

[54] **Park, J. M., Kim, D., Kang, T. G., & Kwon, T.** (2008). Improved serpentine laminating micromixer with enhanced local advection. *Microfluidics and Nanofluidics*, *4*, 513–523. https://doi.org/10.1007/s10404-007-0208-x

[55] **Chung, C. K., Shih, T. R., Wu, B. H., & Chang, C. K.** (2010). Design and mixing efficiency of rhombic micromixer with flat angles. *Microsystem Technologies*, *16*(8), 1595–1600. https://doi.org/10.1007/s00542-009-0980-5

[56] **Sudarsan, A. P., & Ugaz, V. M.** (2006). Fluid mixing in planar spiral microchannels. *Lab on a Chip*, *6*(1), 74–82. https://doi.org/10.1039/B511524H

[57] **Liu, Y., Jiang, D., Wang, S., Cai, G., Xue, L., Li, Y., Liao, M., & Lin, J.** (2022). A microfluidic biosensor for rapid detection of Salmonella typhimurium based on magnetic separation, enzymatic catalysis and electrochemical impedance analysis. *Chinese Chemical Letters*, *33*(6), 3156–3160. https://doi.org/10.1016/j.cclet.2021.10.064

[58] **Wang, Y., Rink, S., Baeumner, A. J., & Seidel, M.** (2022). Microfluidic flow-injection aptamer-based chemiluminescence platform for sulfadimethoxine detection. *Microchimica Acta*, *189*(3), 117. https://doi.org/10.1007/s00604-022-05216-6

[59] **Zhang, Z., Zhao, P., Xiao, G., Lin, M., & Cao, X.** (2008). Focusing-enhanced mixing in microfluidic channels. *Biomicrofluidics*, *2*(1), 014101. https://doi.org/10.1063/1.2894313

[60] **Tran-Minh, N., Karlsen, F., Dong, T., & Le-The, H.** (2014). A Simple and Low Cost Micromixer for Laminar Blood Mixing: Design, Optimization, and Analysis. In T. D. Pham, K. Ichikawa, M. Oyama-Higa, D. Coomans, & X. Jiang (Eds.), *Biomedical Informatics and Technology* (Vol. 404, pp. 91–104). Springer Berlin Heidelberg. https://doi.org/10.1007/978-3-642-54121-6_8

[61] **Niculescu, A.-G., Chircov, C., Bîrcă, A. C., & Grumezescu, A. M.** (2021). Fabrication and Applications of Microfluidic Devices: A Review. *International Journal of Molecular Sciences*, *22*(4), Article 4. https://doi.org/10.3390/ijms22042011

[62] **Ren, K., Zhou, J., & Wu, H.** (2013). Materials for Microfluidic Chip Fabrication. *Accounts of Chemical Research*, *46*(11), 2396–2406. https://doi.org/10.1021/ar300314s

[63] **James, M., Revia, R. A., Stephen, Z., & Zhang, M.** (2020). Microfluidic Synthesis of Iron Oxide Nanoparticles. *Nanomaterials*, *10*(11), Article 11. https://doi.org/10.3390/nano10112113

[64] **Cabeza, V. S.** (2016). High and Efficient Production of Nanomaterials by Microfluidic Reactor Approaches. In X.-Y. Yu (Ed.), *Advances in Microfluidics—New Applications in Biology, Energy, and Materials Sciences*. InTechOpen. https://doi.org/10.5772/64347

[65] **Url-2** < https://pubs.acs.org/doi/full/10.1021/acs.analchem.9b04986>, date retrieved 7.12.2022.

[66] **Martins, J. P., Torrieri, G., & Santos, H. A.** (2018). The importance of microfluidics for the preparation of nanoparticles as advanced drug delivery systems. *Expert Opinion on Drug Delivery*, *15*(5), 469–479. https://doi.org/10.1080/17425247.2018.1446936

[67] **Hwang, J., Cho, Y. H., Park, M. S., & Kim, B. H.** (2019). Microchannel Fabrication on Glass Materials for Microfluidic Devices. *International Journal of Precision Engineering and Manufacturing*, *20*(3), 479–495. https://doi.org/10.1007/s12541-019-00103-2

[68] **Singh, A., Malek, C. K., & Kulkarni, S. K.** (2010). Development in microreactor technology for nanoparticle synthesis. *International Journal of Nanoscience*, *09*(01n02), 93–112. https://doi.org/10.1142/S0219581X10006557

[69] **Shakeri, A., Jarad, N. A., Leung, A., Soleymani, L., & Didar, T. F.** (2019). Biofunctionalization of Glass- and Paper-Based Microfluidic Devices: A Review. *Advanced Materials Interfaces*, *6*(19), 1900940. https://doi.org/10.1002/admi.201900940

[70] **Nishat, S., Jafry, A. T., Martinez, A. W., & Awan, F. R.** (2021). Paper-based microfluidics: Simplified fabrication and assay methods. *Sensors and Actuators B: Chemical*, *336*, 129681. https://doi.org/10.1016/j.snb.2021.129681

[71] **Campbell, S. B., Wu, Q., Yazbeck, J., Liu, C., Okhovatian, S., & Radisic, M.** (2021). Beyond Polydimethylsiloxane: Alternative Materials for Fabrication of Organ-on-a-Chip Devices and Microphysiological Systems. *ACS Biomaterials Science & Engineering*, *7*(7), 2880–2899. https://doi.org/10.1021/acsbiomaterials.0c00640

[72] **Waldbaur, A., Rapp, H., Länge, K., & Rapp, B. E.** (2011). Let there be chip—towards rapid prototyping of microfluidic devices: One-step manufacturing processes. *Analytical Methods*, *3*(12), 2681–2716. https://doi.org/10.1039/C1AY05253E

[73] **Pan, L.-J., Tu, J.-W., Ma, H.-T., Yang, Y.-J., Tian, Z.-Q., Pang, D.-W., & Zhang, Z.-L.** (2018). Controllable synthesis of nanocrystals in droplet reactors. *Lab on a Chip*, *18*(1), 41–56. https://doi.org/10.1039/C7LC00800G

[74] **Rivet, C., Lee, H., Hirsch, A., Hamilton, S., & Lu, H.** (2011). Microfluidics for medical diagnostics and biosensors. *Chemical Engineering Science*, *66*(7), 1490–1507. https://doi.org/10.1016/j.ces.2010.08.015

[75] **Blazej, R. G., Kumaresan, P., & Mathies, R. A.** (2006). Microfabricated bioprocessor for integrated nanoliter-scale Sanger DNA sequencing. *Proceedings of the National Academy of Sciences*, *103*(19), 7240–7245. https://doi.org/10.1073/pnas.0602476103

[76] **Fiorini, G. S., & Chiu, D. T.** (2018, May 30). *Disposable microfluidic devices: Fabrication, function, and application* (London, UK) [Review-article]. Https://Doi.Org/10.2144/05383RV02; Future Science Ltd London, UK. https://doi.org/10.2144/05383RV02

[77] **Iliescu, C., Taylor, H., Avram, M., Miao, J., & Franssila, S.** (2012). A practical guide for the fabrication of microfluidic devices using glass and silicon. *Biomicrofluidics*, *6*(1), 016505. https://doi.org/10.1063/1.3689939

[78] **Mali, P., Sarkar, A., & Lal, R.** (2006). Facile fabrication of microfluidic systems using electron beam lithography. *Lab on a Chip*, *6*(2), 310. https://doi.org/10.1039/b510992b

[79] **Moolman, M. C., Huang, Z., Krishnan, S. T., Kerssemakers, J. W., & Dekker, N. H.** (2013). Electron beam fabrication of a microfluidic

device for studying submicron-scale bacteria. *Journal of Nanobiotechnology*, *11*, 12. https://doi.org/10.1186/1477-3155-11-12

[80] **Faustino, V., Catarino, S. O., Lima, R., & Minas, G.** (2016). Biomedical microfluidic devices by using low-cost fabrication techniques: A review. *Journal of Biomechanics*, *49*(11), 2280–2292. https://doi.org/10.1016/j.jbiomech.2015.11.031

[81] **Strong, M. E., Richards, J. R., Torres, M., Beck, C. M., & La Belle, J. T.** (2021). Faradaic electrochemical impedance spectroscopy for enhanced analyte detection in diagnostics. *Biosensors and Bioelectronics*, *177*, 112949. https://doi.org/10.1016/j.bios.2020.112949

[82] **Randviir, E. P., & Banks, C. E.** (2013). Electrochemical impedance spectroscopy: An overview of bioanalytical applications. *Analytical Methods*, *5*(5), 1098. https://doi.org/10.1039/c3ay26476a

[83] **Barsoukov, E., & Macdonald, J. R.** (Eds.). (2005). *Impedance Spectroscopy: Theory, Experiment, and Applications* (1st ed.). Wiley. https://doi.org/10.1002/0471716243

[84] **Lin, C., Ryder, L., Probst, D., Caplan, M., Spano, M., & LaBelle, J.** (2017). Feasibility in the development of a multi-marker detection platform. *Biosensors and Bioelectronics*, *89*, 743–749. https://doi.org/10.1016/j.bios.2016.10.073

[85] **Dorledo de Faria, R. A., Dias Heneine, L. G., Matencio, T., & Messaddeq, Y.** (2019). Faradaic and non-faradaic electrochemical impedance spectroscopy as transduction techniques for sensing applications. *International Journal of Biosensors & Bioelectronics*, *5*(1). https://doi.org/10.15406/ijbsbe.2019.05.00148

[86] **Daniels, J. S., & Pourmand, N.** (2007). Label-Free Impedance Biosensors: Opportunities and Challenges. *Electroanalysis*, *19*(12), 1239–1257. https://doi.org/10.1002/elan.200603855

[87] **Lin, S.-P., Vinzons, L. U., Kang, Y.-S., & Lai, T.-Y.** (2015). Non-Faradaic Electrical Impedimetric Investigation of the Interfacial Effects of Neuronal Cell Growth and Differentiation on Silicon Nanowire Transistors. *ACS Applied Materials & Interfaces*, *7*(18), 9866–9878. https://doi.org/10.1021/acsami.5b01878

[88] **Park, J., Kim, H., Lee, J.-H., Park, J., Kim, J., Hwang, K., & Lee, B.** (2018). Amyloid Beta Detection by Faradaic Electrochemical Impedance Spectroscopy Using Interdigitated Microelectrodes. *Sensors*, *18*(2), 426. https://doi.org/10.3390/s18020426

[89] **Cheng, I.-F., Yang, H.-L., Chung, C.-C., & Chang, H.-C.** (2013). A rapid electrochemical biosensor based on an AC electrokinetics enhanced immuno-reaction. *The Analyst*, *138*(16), 4656. https://doi.org/10.1039/c3an00190c

[90] **Chiriacò, M. S., Primiceri, E., Montanaro, A., de Feo, F., Leone, L., Rinaldi, R., & Maruccio, G.** (2013). On-chip screening for prostate cancer: An

EIS microfluidic platform for contemporary detection of free and total PSA. *The Analyst*, *138*(18), 5404. https://doi.org/10.1039/c3an00911d

[91] **Team, E.** (2021). PDMS: A review. *Elveflow*. https://www.elveflow.com/microfluidic-reviews/general-microfluidics/the-polydimethylsiloxane-pdms-and-microfluidics/

CURRICULUM VITAE

Name Surname **:** Amenah AL-BARUDI

EDUCATION **:**

- **B.Sc.** **:** 2019, Altinbas University, Faculty of Pharmacy, Department of Pharmacy

PROFESSIONAL EXPERIENCE AND REWARDS:

- 2017- Certificate of High Academic Achievement at Altinbas University.
- 2019- 9 STAR Pharmacist Certificate of Honor at Altinbas University.

PUBLICATIONS, PRESENTATIONS AND PATENTS ON THE THESIS:

- **Amenah Al-Barudi**, Hüseyin KIZIL**.** 2022: Design And Fabrication Of Micromixers For The Efficient Antigen-Antibody Binding. International Graduate Reasearch Symposium- IGRS'22, June 1-3, 2022 Istanbul, Turkey.